DEPARTMENT OF CLINICAL SCIENCES,
DANDERYD HOPSITAL
Division of Cardiology
Karolinska Institutet, Stockholm, Sweden

NOVEL INSIGHTS INTO ECHOCARDIOGRAPHIC ASSESSMENT OF CARDIAC FUNCTION FOLLOWING HEART SURGERY

Nashmil Hashemi

Karolinska Institutet

Stockholm 2018

Cover art by Trinley Dorje. Four Chambers, 2018. Digital Monoprint (1/1) on metallic paper, face-mounted to acrylic panel. tdorjeart.myportfolio.com ©Trinley Dorje

Published by Karolinska Institutet.
Printed by E-print AB, Stockholm, Sweden.

ISBN 978-91-7831-111-8

NOVEL INSIGHTS INTO ECHOCARDIOGRAPHIC ASSESSMENT OF CARDIAC FUNCTION FOLLOWING HEART SURGERY

THESIS FOR DOCTORAL DEGREE (Ph.D.)

By

Nashmil Hashemi

Principal Supervisor:
Associate professor Mahbubul Alam
Karolinska Institutet
Department of Clinical Sciences,
Danderyd Hospital
Division of Cardiology

Co-supervisor(s):
Professor Lars-Åke Brodin
KTH, Royal Institute of Technology
Department of Biomedical Engineering
Division of Medical Engineering

Associate professor Bassem Abdel Samad
Karolinska Institutet
Department of Clinical Sciences,
Danderyd Hospital
Division of Cardiology

Opponent:
Professor Michael Henein
Umeå University
Department of Public Health and Clinical Medicine
Division of Cardiology

Examination Board:
Associate professor Gerhard Wikström
Uppsala University
Department of Medical Sciences
Division of Cardiology, Akademiska Hospital

Professor Torbjörn Ivert
Karolinska Institutet
Department of Molecular Medicine and Surgery,
Division of Cardiothoracic Surgery, Karolinska University Hospital

Associate professor Jens Jensen
Karolinska Institutet
Department of Clinical Science and Education,
Södersjukhuset
Division of Cardiology, S:t Görans Hospital

To my mother for embodying love and determination, and revealing the true meaning of a strong woman

To Janos, Hannah and Julia, my beloved family

ABSTRACT

Assessment of cardiac function is a fundamental in everyday clinical decision making and is essential diagnostic tool for choosing therapy in patients with cardiac disease. Currently, echocardiography is the integral part in management of patients with different cardiac disease and the most established imaging tool in the assessment of cardiac function. Coronary artery bypass grafting (CABG) is an effective treatment in selected patients suffering from advanced coronary artery disease (CAD). Improvement in symptoms, functional status and cardiac function is often used to evaluate the success of CABG. Evaluation of cardiac function often is divided in assessment of systolic and diastolic function. However, systole and diastole are integrated and interconnected parts of cardiac cycle. Thus, a method for quantifying cardiac function which incorporates both systole and diastole is to be preferred. Myocardial performance index (MPI) assessed by pulsed-wave Doppler tissue imaging (PW-DTI) is combining systole and diastole, easy to acquire and is independent of cardiac geometry. The aim of this thesis is to evaluate the feasibility of MPI measured by PW-DTI in assessment of left and right ventricular performance in patients with CAD treated with CABG. In addition, to explore the role of B-type natriuretic peptide (BNP) in predicting long-term major adverse outcomes following CABG and exploring its association with MPI. Finally, this thesis aims to evaluate the impact of conventional aortic valve surgery in comparison to minimally invasive aortic valve surgery (MIAVR) on right ventricular function (RV) assessed by echocardiography.

Methods and Results

Study I, forty six patients who were accepted for CABG were included. They all were investigated by dobutamine stress-echocardiography (DSE) prior to CABG and 3 month after CABG. Several methods for evaluation of left ventricular systolic and diastolic function had been applied, i.e. EF, longitudinal systolic and diastolic velocities as well as MPI. All the measurements were performed at rest and at peak DSE. The values from pre-CABG were compared to those after CABG. At baseline, MPI was prolonged both at rest (0.61 ±0.13) and at peak DSE (0.78±0.16). Accordingly, ejection fraction (EF) was also impaired at rest (42.7±8%) and at peak DSE (49.2±9). Similarly, wall-motion score index WMSI was impaired at rest (1.1±0.2) and at peak DSE (1.4±0.2). After CABG, MPI improved significantly both at rest

(0.45±0.08; P < 0.001) and at peak DSE (0.56±0.1; P < 0.001). On the other hand, EF and WMSI did not improve at rest (43.7±8% and 1.1±0.2, respectively). However, at peak DSE an improvement of both EF (54.2±9; P < 0.05) and WMSI (1.1±0.16; P < 0.001) was observed.

Study II The same patient cohort as in study I was used for analyzing the impact of CABG on RV function. Coronary angiography, DSE and exercise bicycle test were performed 1 month before and 3 months after CABG. Right ventricular index of myocardial performance (RIMP), right ventricular systolic velocity (RVS) and displacement (TAPSE) at the lateral tricuspid annulus were all assessed. The RIMP improved following CABG both at rest (0.45 ± 0.11 vs. 0.38 ± 0.08 CABG, P = 0.013) and during DSE (0.75 ± 0.23 vs. 0.49 ± 0.14, P < 0.001). Compared to baseline, TAPSE reduced substantially after CABG both at rest (23.9 ± 4.46 vs. 14.6 ± 3.67, P < 0.001) and during DSE (20.9 ± 4.16 vs 11.9 ± 3.60, P < 0.001). A significant decline in RVS was also observed following CABG both at rest (11.9 ± 2.40 vs. 8.5 ± 1.93, P < 0.001) and during DSE (15.6 ± 4.30 vs. 10.5 ± 3.21, P < 0.001). On contrary, compared to pre-CABG values exercise capacity improved significantly following CABG (128.4 ± 40.12W vs 142.1 ± 46.73 W, P = 0.014).

Study III was a predefined post hoc analysis of CMILE study (Cardiac Function after Minimally Invasive Aortic Valve Implantation including 40 patients with severe aortic stenosis and eligible for isolated aortic valve replacement. The patients were randomized 1:1 either to conventional aortic valve replacement (AVR) or minimally invasive aortic valve replacement (MIAVR). The impact of these two surgical techniques on right ventricular mechanics and contractility was evaluated by echocardiography. Compared to baseline RV strain rate (RV-LSR) was preserved after MIAVR (-1.52±0.5 vs -1.49±0.4 1/s, p=0.84) but declined following AVR (-1.67±0.3 vs -1.38±0.3 1/s, p<0.01). RV longitudinal strain (RV-LS) was deteriorated after AVR (-27.4±2.9% vs -18.8±4.7%, p<0.001) and MIAVR (-26.5±5.3% vs -20.7±4.5%, p<0.01). Peak systolic velocity of the lateral tricuspid annulus (RVS) declined by 18.8% in the MIAVR group (10.1±2.9 vs 8.2±1.4 cm/s, p<0.01) and 36.6% in the AVR group (9.3±2.1 vs 5.9±1.5 cm/s, p<0.01) when values from before surgery were compared to after surgery.

In Study IV, 99 patients with CAD who underwent CABG were evaluated by a biomarker BNP and Echocardiography. In a subpopulation of 40 patients

DTI and MPI were obtained. Patients were followed-up for 5 years and during this period death, myocardial infarction, stroke and hospitalization due to heart failure were recorded. The role of postoperative BNP for predicting major outcomes was assessed and its association with MPI was determined. Seventeen patients experienced major adverse outcomes during the follow-up. Univariate analysis revealed that creatinine clearance ($P<0.01$), body mass index (BMI, $P<0.01$), postoperative BNP ($P<0.001$) and preoperative LV-MPI ($P=0.04$) were all significantly associated with major outcomes at follow-up. However, after correcting for cofactors in multivariate analysis only postoperative BNP ($P=0.003$) and BMI ($P=0.025$) were associated with major outcomes.

CONCLUSIONS: Myocardial performance index and right ventricular index of myocardial performance improved significantly following CABG in patients with CAD both at rest and peak DSE and appear to be a sensitive measure of myocardial function in patients with CAD. Postoperative BNP obtained in a stable clinical condition, 3 month after CABG is a predictive of major outcomes 5 years after CABG. Load-independent contractility is preserved following MIAVR but reduced following AVR. Load-dependent measures of myocardial function all declined following both MIAVR and AVR however, to a much lesser extent following MIAVR.

LIST OF SCIENTIFIC PAPERS

I. **Hashemi N**, Hedman A, Abdel Samad B, Brodin L-Å, Alam M

Feasibility of myocardial performance index for evaluation of left ventricular function during dobutamine Stress echocardiography before and after coronary artery bypass grafting.
Echocardiography. 2014; 31: 989-995

II. **Hashemi N**, Hedman A, Abdel Samad B, Brodin L-Å, Alam M

Improved right ventricular index of myocardial performance in the assessment of right ventricular function after coronary artery bypass grafting.
Interactive Cardiovasc Thoracic Surgery. 2018; 26: 798-804

III. **Hashemi N**, Johnson J, Brodin L-Å, Gomes-Bernardes A, Sartipy U, Svenarud P, Dalén M, Bäck M, Alam M, Winter R

Right ventricular mechanics and contractility after aortic valve replacement surgery: a randomised study comparing minimally invasive versus conventional approach
Open Heart. 2018; 5(2):e000842.

IV. **Hashemi N**, Brodin L-Å, Alam M, Abdel Samad B

Predictive value of B-type natriuretic peptide following coronary artery bypass grafting and its association with myocardial performance index.
Manuscript

CONTENT

LIST OF ABBREVIATIONS

A	Late diastolic inflow velocity
A´	Late diastolic longitudinal annular velocity
ACEI	Angiotensin-converting enzyme inhibitors
ARB	Angiotensin II receptor blocker
AS	Aortic stenosis
AVR	Aortic valve replacement surgery
BMI	Body mass index
BNP	B-type natriuretic peptide
CAD	Coronary artery disease
CHF	Congestive heart failure
CI	Confidence interval
CMILE	Cardiac function after minimally invasive aortic valve implantation
CW	Continuous wave
CX	Circumflex artery
DAPP	Dynamic adaptive piston pump
DTI	Doppler tissue imaging
E	Early diastolic inflow velocity
E´	Early diastolic longitudinal annular velocity
ECG	Electrocardiogram
EDA	End diastolic area
EDD	End diastolic diameter
EDV	End diastolic volume
EF	Ejection fraction
ESA	End systolic area
ESD	End systolic diameter
ESV	End systolic volume
ET	Ejection time
FAC	Fractional area change
GLS	Global longitudinal strain

ICT	Isovolumic contraction time
IVRT	Isovolumic relaxation time
LA	Left atrium
LAD	Left anterior descending artery
LS	Longitudinal strain
LSR	Longitudinal strain rate
LV	Left ventricular
MACE	Major adverse cardiovascular events
MI	Myocardial infarction
MIAVR	Minimally invasive aortic valve replacement surgery
MPI	Myocardial performance index
OR	Odds ratio
PASP	Pulmonary systolic arterial pressure
PEP	Pre-ejection period
POP	Post-ejection period
PW	Pulsed wave
RA	Right atrium
RCA	Right coronary artery
RIMP	Right ventricular index of myocardial performance
ROC	Recipient operator curve
ROI	Region of interest
RV	Right ventricular
RVD1	Basal RV linear dimension
RVOT	RV outflow diameter
S	Peak systolic velocity
SPAP	Systolic pulmonary artery pressure
STE	Speckle tracking echocardiography
SV	Stroke volume
TAPSE	Tricuspid annular plane systolic excursion

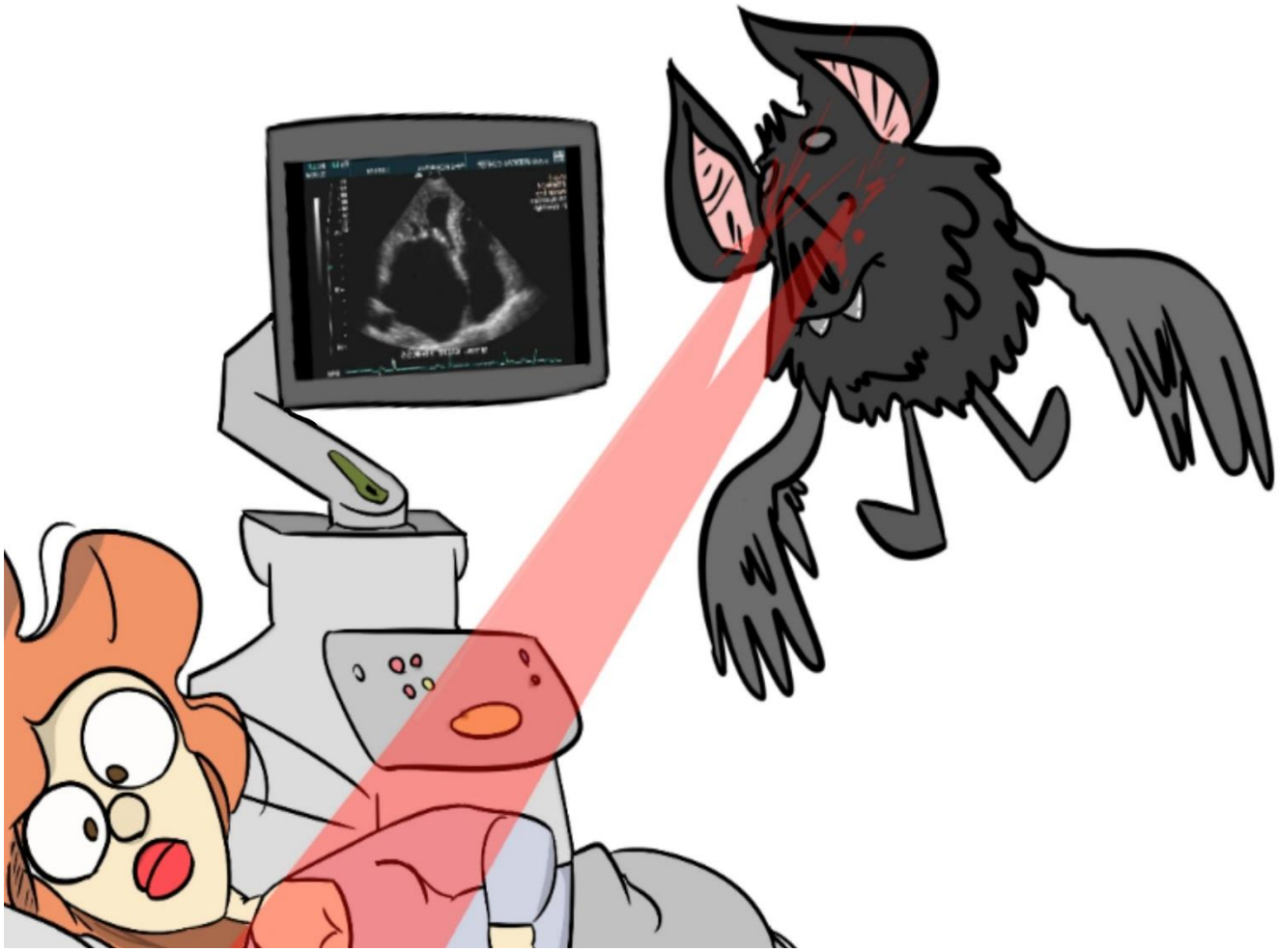

To my daughters.

1 INTRODUCTION

1.1 EVOLUTION OF ECHOCARDIOGRAPHY,

USING SOUND TO VISUALIZE STRUCTURES

The history of echocardiography stands out as a proof for human inquisitiveness, curiosity, ingenuity and collaboration across fields of science. Ultrasound and doppler are common phenomenon in nature. Bats, which are blind mammals, use ultrasound to navigate when flying and form a “sonic image” of their environment. The phenomenon was first described by L. Spallanzani in YEAR (1729-1799). With the discovery of piezoelectricity by the Curie brothers (1), a new era of scientific investigations emerged. The technology was used in reflectoscopes to detect flaws in industrial metals. The development of the reflectoscope was accelerated during World War II as naval sonar was used for military purpose. The medical use of cardiac ultrasound emerged in the 1950s as a result of a fruitful cooperation between Inge Edler, a cardiologist, and Carl Hellmuth Hertz, a physicist (Fig.1), both from Lund, Sweden (2). At the time, the severity of mitral stenosis was evaluated by invasive catheter measurements. Inge Edler aimed to acquire accurate measurements of mitral stenosis prior to surgery, for which he partnered with Carl Hellmuth Hertz to find a solution. The turning point came when Hertz borrowed a reflectoscope from Siemens and performed the first echocardiography on himself. He identified a signal that moved with cardiac motion. Using M-mode, Edler and Hertz developed the technique further to evaluate the mitral valve. Since the introduction of M-mode echocardiography, technological development has been sustained with consistent improvements in image quality and evolving new modalities. For the past decades echocardiography has undergone a particularly dynamic phase of development. Today, echocardiography is an integral part of clinical cardiology.

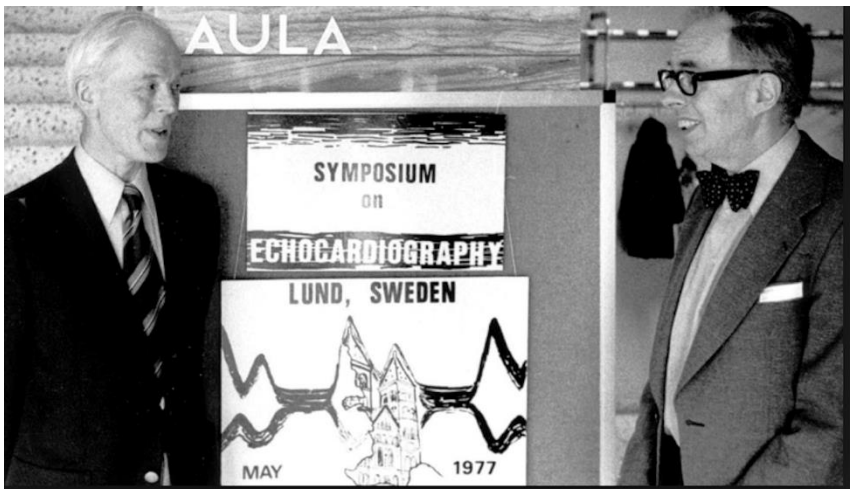

Figure 1. Inge Edler and Hellmuth Hertz (Image from“Sydsvenska medicinhistoriska sällkapet” photo archive)

1.2 DIFFERENT ECHOCARDIOGRAPHIC TECHNIQUES

1.2.1 One and two dimensional echocardiography

One-dimensional M-mode echocardiography was the first echocardiographic examination performed by Inge Edler and Hellmuth Hertz in 1953. The technique was revolutionizing the cardiac examination of patients with mitral stenosis. Later, M-mode echocardiography was further developed and was used in measuring cardiac dimensions and valvular function. Although, M-mode echocardiography has an excellent temporal resolution it has the disadvantage of being one-dimensional. Later, linear mechanical scanners were designed (Fig.2) allowing visualization of a two-dimensional (2D) image of the heart. Eventually, sector scanners were developed with further improving image quality.

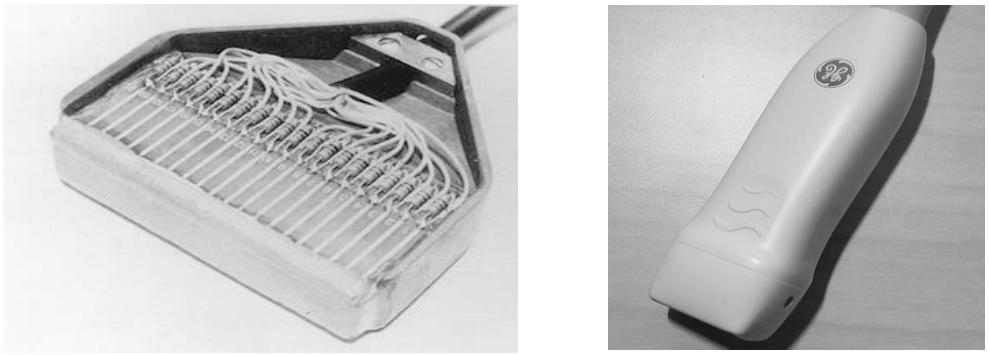

Figure 2. A multielement transducer that provides an electronic linear scan to represents the first real-time, 2D, echocardiography (Left image, with permission: Circulation; 1996; 93 (7): 1321-1327) and a modern sector scanner transducer (Right).

With additional improvement of 2D echocardiography and using different projections, a comprehensive assessment of cardiac structures and function can be achieved. Currently, 2D echocardiography (Fig 3) is the backbone of echocardiographic examination allowing evaluation of cardiac geometry, size, volume and function. These measurements have tremendous impact on management, diagnosis, and prognosis of patients with a variety of cardiac disease (3).

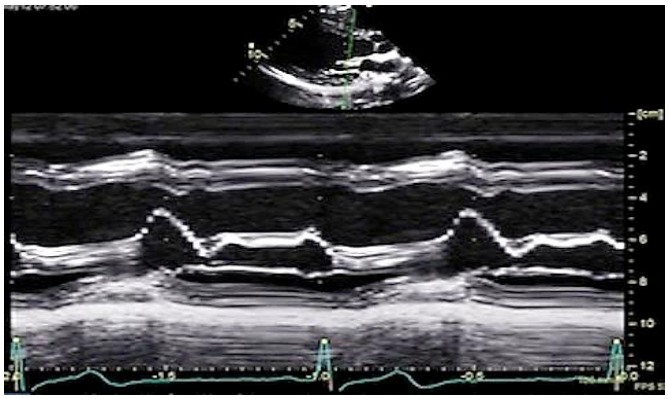

Fig. 3 One-dimensional M-mode echocardiography of mitral valve.

1.2.2 Doppler echocardiography

Christian Doppler was the first one who described the Doppler principle in 1842 when he tried to describe the shift in the color of starlight. The Doppler principle implies that frequency of sound waves is higher when the source of sound moves toward the observer and lower if the sound source moves away from the observer. In the circulatory system, the moving targets are the red blood cells (RBC). According to the Doppler effect, the frequency of reflected ultrasound waves is higher when the RBCs move toward the transducer and lower when they move from the transducer. This frequency shift is used in Doppler echocardiography to calculate the velocity of moving red blood cells (RBC) in the circulatory system (4). One important limitation of Doppler echocardiography is its angle dependency. The maximum velocity of RBCs is underestimated if the angle of interrogation (θ) exceeds 20°.

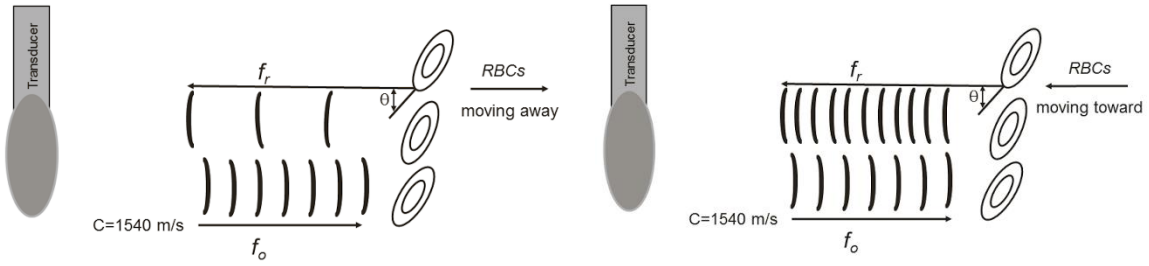

Figure 4. Illustration showing the Doppler effect in the circulatory system. RBCs: red blood cells; θ: the angle between the ultrasound wave and RBC; C: speed of ultrasound in blood (1540 m/s).

In clinical practice, different modalities of Doppler echocardiography are applied for measuring cardiac flow: i) Continuous wave Doppler (CWD). It refers to continuous transmission of ultrasound waves towards the red blood cells and continuous receiving of the reflected waves from moving red blood cells; ii) In the Pulsed wave Doppler (PWD) mode, a single crystal sends and receives the reflected ultrasound waves; and iii) Color Doppler flow imaging which is based on a rapid, multigated PWD with color coding superimposed on the grey-scale 2D image. Red corresponds to flow towards and Blue corresponds to flow from the transducer. Doppler echocardiography is the backbone of noninvasive assessment of cardiac hemodynamics.

1.2.3 Doppler tissue imaging

Doppler tissue imaging (DTI) is an echocardiographic technique that applies Doppler principles for visualizing the motion of myocardial tissue, thus allowing measurement of myocardial tissue velocities (Fig. 5). In this technique, color mode is superimposed on the grey-scale 2D image (5). The

color-coding is similar to that of flow Doppler mode with Red moving towards and Blue moving away from the transducer. The velocity of myocardial tissue is much lower than the velocity of red blood cells, but the amplitude of the reflected waves is much higher, thus requiring higher frame rates that are usually >100 frame rate/s (6). The recordings can be stored digitally for further off-line analysis, which allows measurement of i) tissue velocity; ii) Myocardial displacement; and iii) deformation analysis. The myocardial velocities can be measured using either Color DTI or pulsed wave (PW) DTI. PW-DTI yields high temporal resolution but does not allow analysis of multiple myocardial segments simultaneously. Myocardial velocities obtained by color DTI are somewhat lower than the velocity measured by PW-DTI. It has been proposed that PW-DTI might overestimate myocardial tissue velocities due to spectral broadening (7).

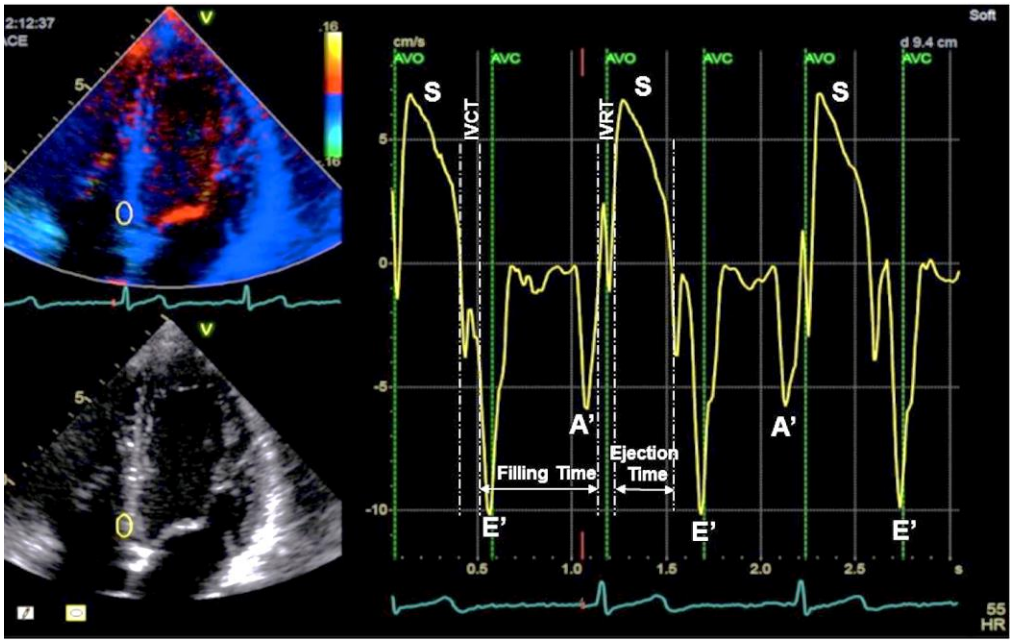

Figure 5. Tissue velocities and cardiac time intervals by color-DTI. AVO: Aortic valve opening; AVC: Aortic valve closure; IVCT: Isovolumic contraction time; IVRT: Isovolumic relaxation time; E' and A': peak early and late annular longitudinal tissue velocity; S: peak systolic annular longitudinal tissue velocity.

1.2.3.1 Myocardial velocities

DTI allows measuring peak myocardial tissue velocities (8), and is particularly well suited for the measurement of myocardial motion along the long axis of the ventricular walls. Myocardial velocities can be measured from any segment of the ventricular walls; however the most common sights for obtaining systolic and diastolic velocities are at the level of mitral and tricuspid annulus in apical four-chamber view. From DTI recordings the

following parameters could be obtained: i) IVC (Isovolumic contraction phase), a biphasic phase representing slight longitudinal shortening before ventricular ejection- IVV (peak myocardial velocity during IVC) ; ii) S (peak systolic velocity); measured as the peak positive value during the ejection period; iii) IVR (Isovolumic relaxation phase), a negative peak representing slight longitudinal elongation before onset of ventricular filling; iv) E´ (Early diastolic velocity) measured as a negative diastolic peak. Mitral E´ is a good indicator of LV myocardial relaxation. It is one of the main parameters in noninvasive assessment of LV filling pressure; and v) A´ (Late diastolic velocity), which is measured as a negative diastolic peak and coincides with atrial contraction (Fig. 5).

1.2.3.2 Cardiac time intervals

From Color DTI or Pulsed DTI, different time intervals of the cardiac cycle can be obtained (8): i) IVCT (Isovolumic contraction time) corresponds to the time interval between A-wave ending of preceding cardiac cycle to S-wave beginning of the next cardiac cycle; ii) ET (Ejection time) is measured as the duration of S-wave; and iii) IVRT (Isovolumic relaxation time) is measured from S-wave ending to the beginning of A´-wave (Fig.5).

1.2.4 Speckle tracking echocardiography

Speckles are produced by interference, scattering and reflection of ultrasound beams in the myocardium. Speckle tracking echocardiography (STE) measures myocardial Strain (S) by tracking the speckles throughout the myocardium. Hence, strain is a measure of myocardial deformation. STE is angle-independent since it relies on tracking the speckles in two dimensions throughout the myocardium, in the direction of myocardial fibers and not along the ultrasound beam. Strain is defined as the magnitude of the changes in the length of myocardial fibers relative to their baseline length. It is is calculated as follows $S\ (\%) = (L_t - L_0)/L_0$, where L_t is the myocardial fiber length at time $_t$ and L_0 is the myocardial fiber length at baseline (9). Myocardial strain rate (SR) is the speed of the changes in the length of myocardial fibers. Myocardial strain can be measured along the longitudinal fibers (longitudinal strain), circumferential myocardial fibers (circumferential strain), and radial fibers (radial strain), (Fig 6). Longitudinal S/SR are measured in apical views. Accordingly, circumferential and radial strain are be obtained from parasternal short axis views.

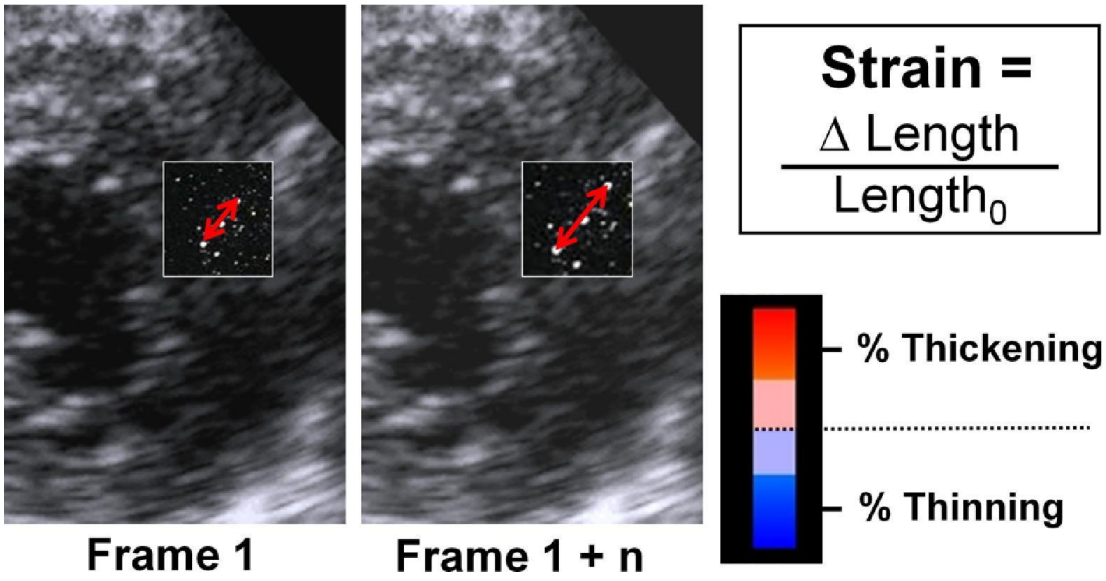

Fig.6 Assessment of 2-dimensional strain by speckle tracking echocardiography in short axis view (above). Orientation of myocardial fibers in the left ventricle and different vectors of myocardial strain (below) Reprinted from Gorcsan et al; JACC 2011; 58 (14): 1401-1413, with permission from Elsevier.

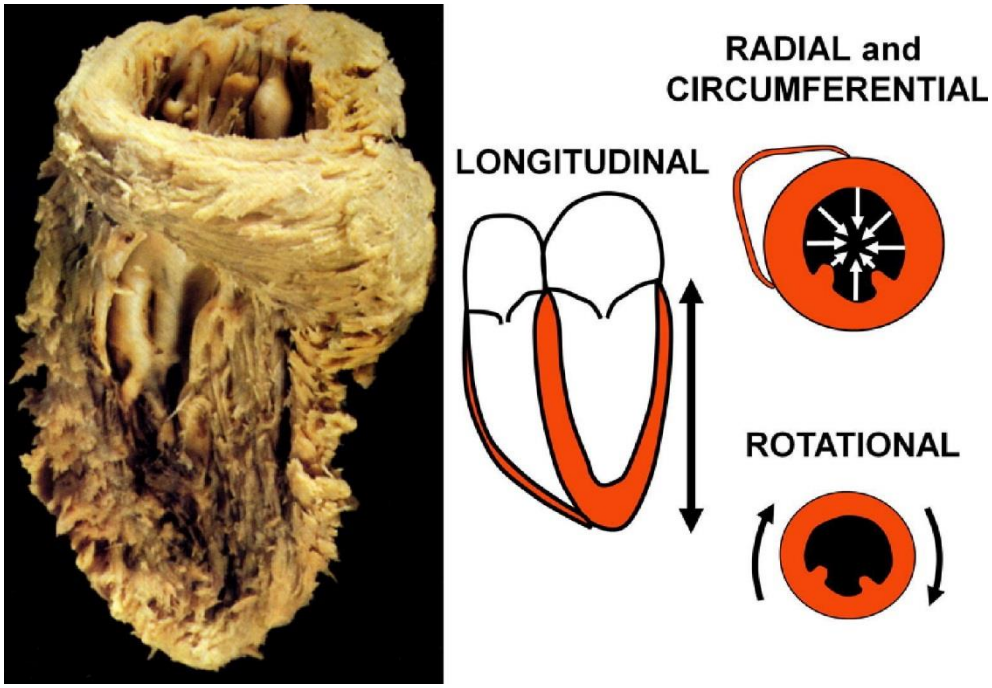

1.3 LEFT VENTRICLE

LV myocardium is approximately 2-3 times thicker than RV myocardium. LV function resembles a pump, receiving blood from the left atrium (LA) during diastole and ejecting blood into the systemic circulation during systole. The LV chamber is divided into functionally two major areas: the inflow tract and the outflow tract.

The inflow tract consists of the mitral apparatus. The LV outflow tract is a narrow cavity between the interventricular septum (anteriorly) and the anterior mitral leaflet and the aortic orifice (posteriorly).

1.3.1 Left ventricular architecture

Myofiber orientation of the heart architecture was first described more than 500 years ago as 2 spiral bands warping around the apical vortex (10). More recently, it has been further developed by Torrent-Guasp (11). He described a muscular band running from the root of pulmonary artery to the root of aorta, forming a helix in the space (Fig.7). The band is forming a basal loop consisting of circumferential transverse fibers which occupy the base and the upper septum and surrounds both ventricles. It can compresses and rotate. A helix which consists of 2 oblique bands; a right-handed or counterclockwise coil descending from the basal loop to the apex; and a left-sided or clockwise coil ascending from the apex to the basal loop (12). The myocardial fibers of the descending band contract at the opposite direction of the ascending band. This description of the heart architecture has changed our view of LV function, which was understood to be compression during systole in order to eject blood and dilating during diastole to receive blood. The helical model describes several motions of during systole and diastole: i) contraction of the basal loop which corresponds to isovolumic systole; ii) contraction of descending band leading to the clockwise twisting of the base and the counterclockwise twisting of the apex, during this period the myocardial fibers are thickening and shortening causing ejection; iii) contraction of the ascending band starts after the contraction of the descending band and stays longer. Thus when the myocardial fibers of the descending band stop contracting the contraction of myocardial fibers of the ascending band leads to lengthening of the LV, creating a course for suction of blood in early diastole.

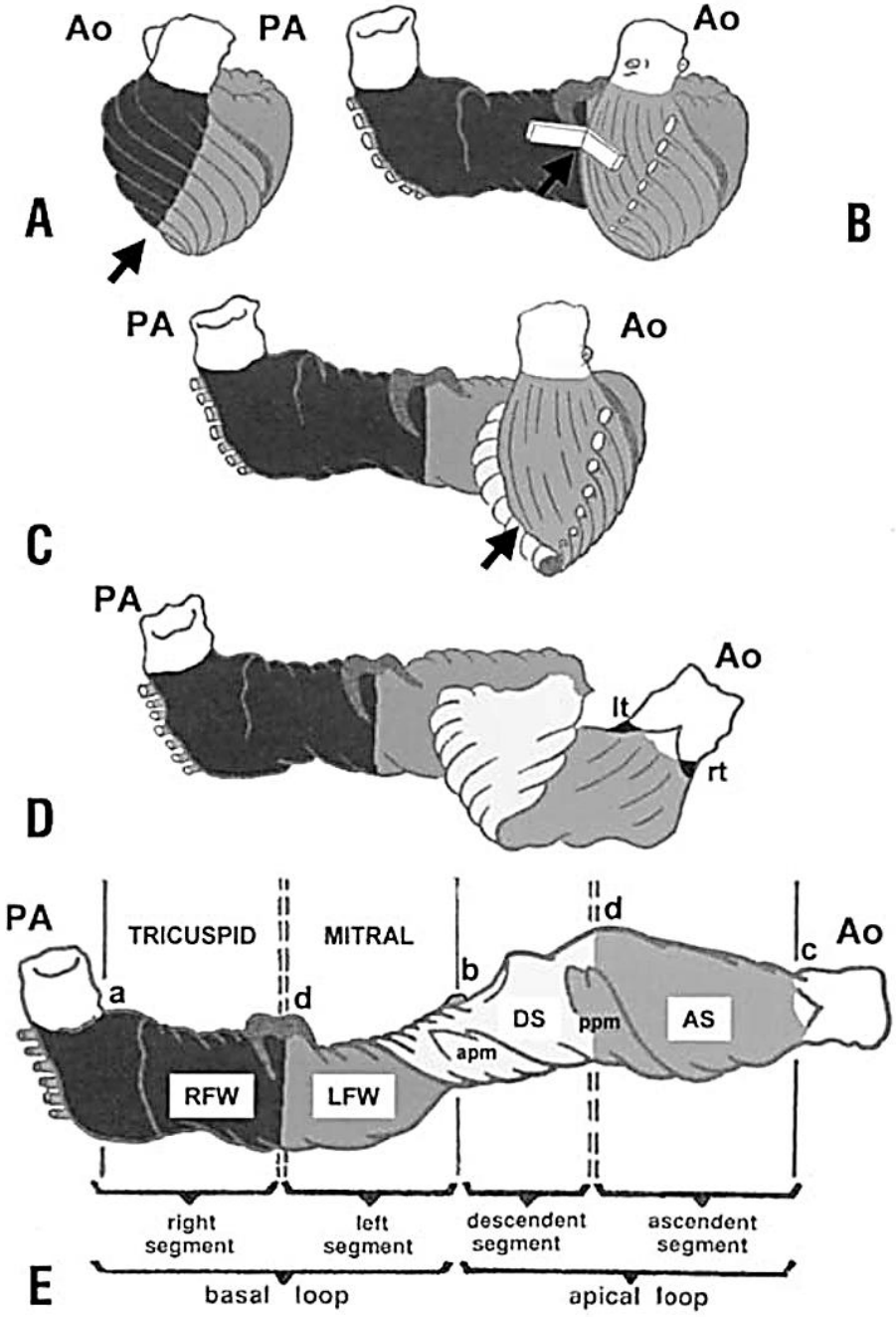

Figure 7. Illustration of dissection of the ventricular myocardial band according to Torrent-Guasp (11). apm: anterior papillary muscle; AS: ascending segment; ppm: posterior papillary muscle; Ao: aorta; DS, descending segment; LFW, left ventricular free wall; lt: left trigone of the aorta; PA: pulmonary artery; ppm: posterior papillary muscle; RFW: right ventricular free wall; rt: right trigone of the aorta. (Reproduced with permission from "The Journal of Thoracic and Cardiovascular Surgery"; 2001; 122 (2): 389-392.

1.3.2 Ejection fraction

EF is the most widely used echocardiographic modality for evaluation of LV systolic function. It could be assessed qualitatively (visually) as referred to "Eye balling" or can be quantified using the biplane summation of disks (modified Simpson's biplane). EF is calculated from LV volumes as (EDV-ESV)/EDV (9). The principle underlying Simpson's biplane rule is that the LV volume is the summation of volumes of a stack of elliptical discs. Apical four-chamber and 2-chmaber views are acquired to asses LV volumes. In order to assess LV volumes the interface between the myocardium and the LV cavity is traced and the tracing is closed at the level of mitral annulus. The volume calculation is based on the assumption that LV is elliptical-shaped. Despite several limitations, it is best validated as a prognostic marker. Several studies have confirmed EF as a predictor of outcomes in heart failure (HF) and as a predictor of sudden cardiac death (13)

1.3.3 Systolic myocardial velocities

Systolic myocardial velocities at the level of mitral annulus have been shown to be a good measure of myocardial longitudinal function which are well-correlated with LVEF and LV dp/dt (14). Tissue velocities can be used to quantify myocardial function in patients with CAD however, with important limitations. In mild CAD, the velocity of "S" is decreased. However, in moderate CAD "S" remains positive. On the other hand, it has been shown that myocardial velocities are more appropriate markers of regional myocardial function in severe ischemia (15). In normal ventricles, IVC is dominated with a brief positive spike. During severe ischemia, IVC spike becomes negative. Additionally, it has been shown that, in patients with diastolic heart failure, the amplitude of mitral annular peak systolic velocity is lower compared to age-matched healthy controls (16). Several studies have confirmed the prognostic role of systolic myocardial velocities in patients with heart failure and CAD (17).

1.3.4 Global Longitudinal strain

Global longitudinal strain (GLS) is the most commonly used strain-based modality in everyday clinical practice. GLS can be assessed using DTI (18)or STE (19). However, assessment of GLS using STE is preferred since STE is angle-independent and DTI is angle-dependent. (20). GLS is calculated as an average of regional longitudinal strain measured in 3 standard apical views namely, apical long axis, four-chamber and two-chamber views (21). One of

the limitations of the current technique in assessment of strainthe relatively high variability between different vendors (20). The normal reference values for GLS can vary depending on which vendor is when assessing GLS (22).

1.3.5 Left ventricular diastolic function

LV diastolic function was first evaluated invasively using the rate of LV pressure reduction, LV relaxation time constant, and measurement of myocardial and chamber stiffness (23). Currently, noninvasive echocardiographic assessment of diastolic function is used in everyday clinical practice (Fig.8). It incorporates PW-Doppler of mitral inflow, mitral annular myocardial velocities assessed by PW-DTI, LA volume, and measurement of pulmonary systolic artery pressure (PASP). The current guidelines for evaluation of diastolic function also take EF into consideration (24). One of the aims of the current guidelines is echocardiographic estimation of LV filling pressure.

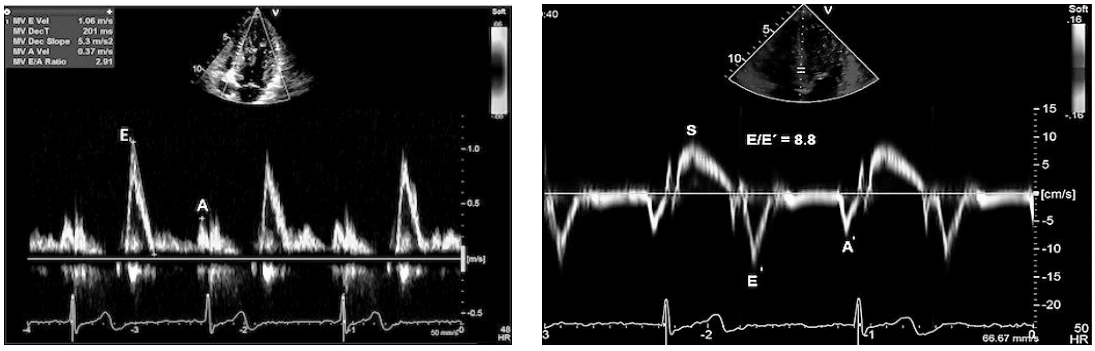

Figure 8. Evaluation of LV diastolic function; mitral inflow pattern (left); E´ velocity (right): E and A: early and late mitral inflow velocity; E' and A': peak early and late annular longitudinal tissue velocity; S: peak systolic annular longitudinal tissue velocity.

1.3.6 Cardiac time intervals a historical perspective

In the late 1960s indirect measurement of systolic time intervals was performed by simultaneous recordings of (1) electrocardiogram (ECG); 2) phonocardiogram, from the area with the loudest aortic component of the second heart sound; and (3) indirect carotid pulse tracing, using a funnel-shaped sensing head connected to the transducer by air-filled tube, and manually held over one carotid artery (25). The total electromechanical systole (QS_2) was defined as the interval from the onset of QRS on the ECG to the closure of aortic valve (S_2) as reflected as the second heart sound on the phonocardiogram. Ejection time (ET) was measured from the beginning upstroke to the trough of incisura of carotid pulse tracing. The interval

between the first (S_1=closure of AV valves) and the second heart sound (S_2 =closure of the semilunar valves) was also measured-S_1S_2 (Fig. 9). The following time intervals were calculated: Pre-ejection period (PEP)=QS_2 -ET and Isovolumic contraction time (ICT)=S_1S_2 -ET were calculated (26). Subsequently, high-speed recordings of aortic valve movements by echocardiography was used as an alternative method for determination of the systolic time intervals (Fig. 9) Several studies demonstrated that diminished ET, a high ratio of pre-ejection period (PEP)/ET, and a prolonged isovolumic relaxation time (IVRT) were associated with left ventricular dysfunction (27, 28).

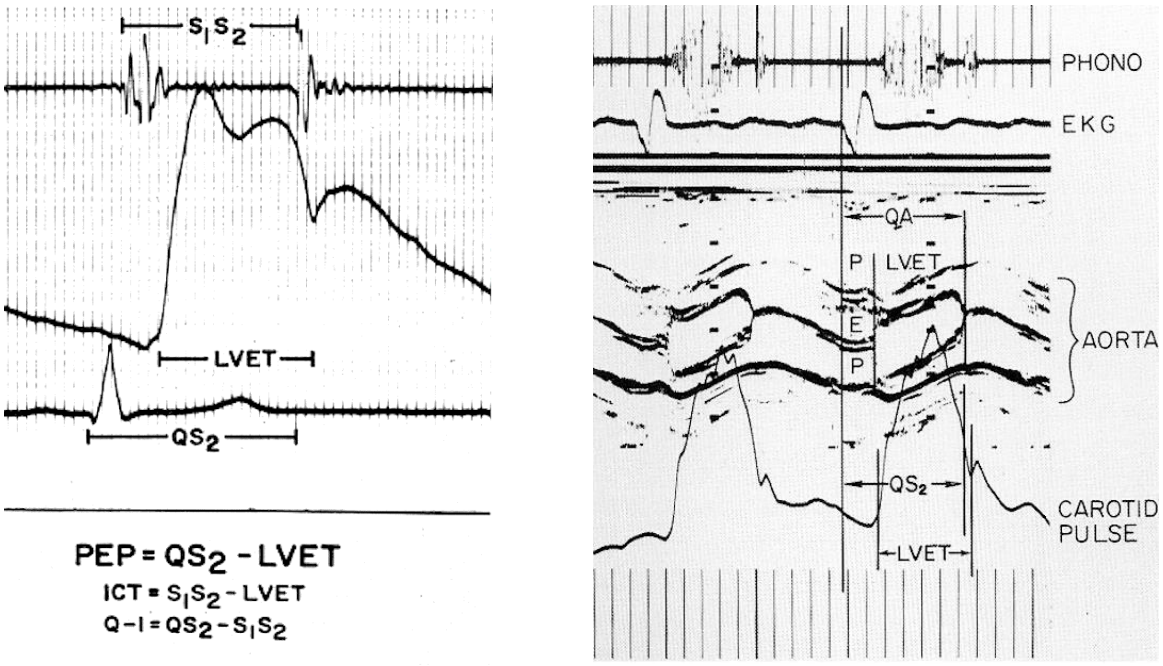

Figure 9. Measuring systolic time intervals by simultaneous carotid arterial pulse tracing, ECG and phonocardiogram (left. Reproduced with permission from Weissler AM. et al Circulation. 1968; 37 (2):149-59). Determination of systolic time intervals using phonocardiogram, ECG, M-mode echocardiography of aortic valve, and indirect carotid arterial pulse tracing (right). PEP: Pre-ejection period; QS2: total electromechanical systole; LVET: left ventricular ejection time; S_1S_2: heart sounds interval; Q-1: interval from onset of QRS to first heart sound; ICT: isovolumic contraction time (Reproduced with permission from Miltiadis A. et al; Circulation; 1975; 51(2):114-17).

1.3.7 Myocardial performance index a historical perspective

Earlier studies had mainly focused on measuring systolic time intervals as described previously. The myocardial performance was quantified using the ratio of PEP/ET (27, 29). Using the ratio would overcome limitation of the cardiac time intervals in the presence of arrhythmia. Further, investigators subdivided the PEP into the electromechanical delay and ICT which was associated with contractility (23). It was technically difficult and complicated to obtain the Isovolumetric time intervals before the era of Doppler echocardiography. However, with the evolvement of echocardiography, the time intervals of the cardiac cycle could easily be obtained. ICT and Isovolumetric relaxation time (IVRT) have long been used in assessment of systolic- and diastolic function, respectively (30, 31).

It had been demonstrated that the ratio of (PEP)ICT/ET provides a useful index which correlates well with stroke volume, cardiac output and fractional shortening (26). Later, it was shown that an index of myocardial relaxation is frequently prolonged in patients with cardiac disease (32). Subsequently, Mancini et al (28) demonstrated that isovolumic index, which they described a ratio of the sum ICT and IVRT divided by ET, is a sensitive marker of myocardial dysfunction (33). The index was assessed by simultaneous measurement of carotid artery pulse tracing and mitral M-mode echocardiogram .

1.3.8 Myocardial performance index by Doppler flow echocardiography

In 1995, Tei and his colleagues introduced a new Doppler index of combined systolic and diastolic myocardial performance (34). Patients with dilated cardiomyopathy with moderately and severely reduced EF were compared with healthy subjects. PW-DTI of mitral inflow pattern and PW-DTI of left ventricular outflow pattern was used for measuring different cardiac time intervals. Different time intervals were measured. Then the “new index of myocardial performance” was assessed as the ratio of (ICT+IVRT)/ET (34); (Fig 10). Ventricular dysfunction results in the prolongation of both ICT and IVRT and in a reduction of ET. Therefore, myocardial performance index is increased in patients with ventricular dysfunction (35). Tei et al showed that the normal range for LVMPI was (0.39 ± 0.05) in healthy persons; (0.59 ± 0.1) in patients with moderate heart failure and (1.06 ± 0.24) in patients with severe heart failure (23). Subsequent studies from the same investigators showed good correlation between the MPI and invasive measurements of systolic LV performance (peak +dP/dt) and diastolic LV performance (peak -dP/dt), and tau by left ventricular catheterization (23).

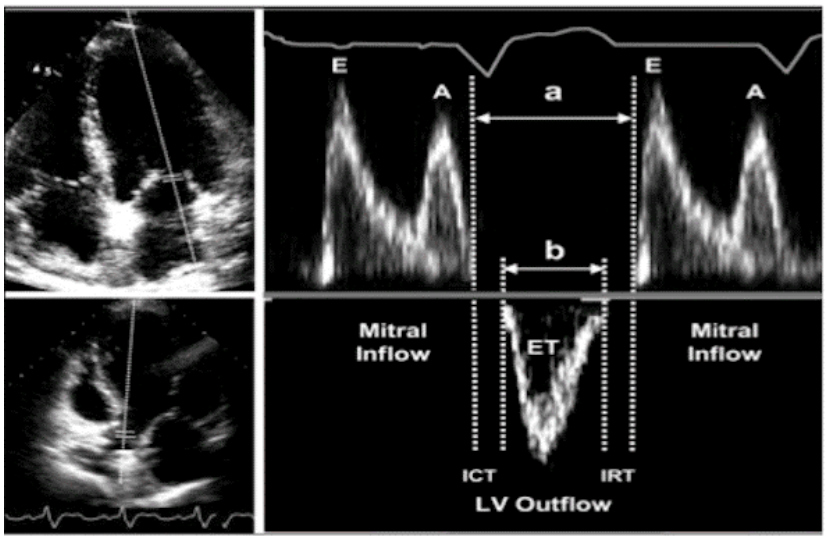

Figure 10. Assessment of left ventricular myocardial performance from mitral inflow and left ventricular (LV) outflow.

Similarly, right ventricular index of myocardial performance (RIMP) can be assessed using Doppler recordings of tricuspid inflow pattern and right ventricular outflow pattern. (Fig. 11)

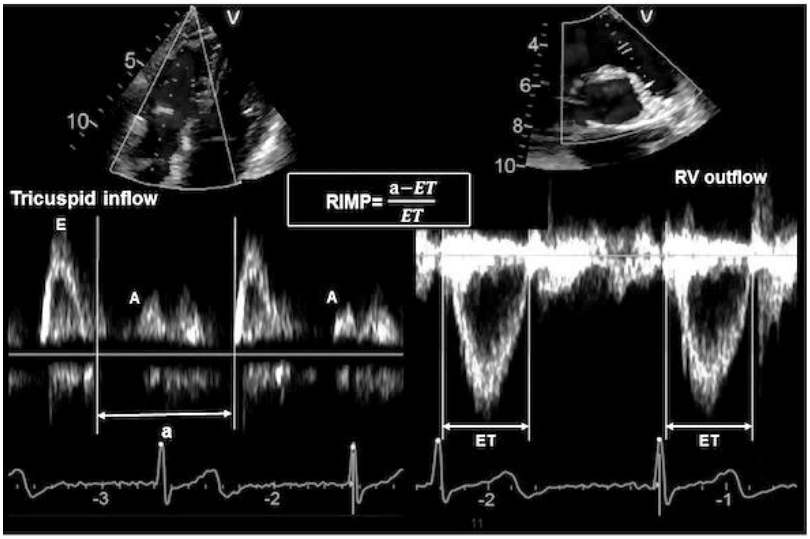

Figure 11. Assessment of right ventricular index of myocardial performance (RIMP) using tricuspid inflow and right ventricular (RV) outflow. ET: Ejection time.

1.3.9 Myocardial performance index by Doppler tissue echocardiography

Recently assessment of MPI by color DTI or pulsed DTI (Fig.) has evolved, allowing measurement of all time intervals from the same heart cycle (36). However, assessment of MPI by Doppler flow echocardiography has the disadvantage of measuring time intervals from two different heart cycles, which could compromise accuracy in significant arrhythmias and varying RR-interval on ECG. Conventional MPI, assessed by pulsed-Doppler, is preload-dependent while MPI assessed by DTI is less dependent in preload (37, 38).

Additionally, assessment of MPI by pulsed DTI is accurate and reproducible because it has high temporal resolution and is easy to obtain. A good correlation between MPI obtained with DTI and MPI determined by pulsed DTI has, previously been confirmed by several studies. Accordingly, a good correlation between tissue Doppler MPI and pulsed-Doppler MPI has been demonstrated(39). Although only mild agreement between PW-DTI and conventional pulsed-Doppler MPI has been shown, high accuracy of both methods in detection of ventricular dysfunction has been demonstrated. Accordingly, higher cut-off values for MPI assessed by PW-DTI has been suggested (40). More recently, assessment of MPI by DTI M-mode through mitral valve leaflets has evolved (41), which has shown to have strong association with invasive measurements of cardiac function (42).

1.3.10 Cardiac state diagram

Cardiac State Diagram (CSD), (43) is a new modality for displaying different cardiac events and cardiac time intervals in a simple and intuitive graphical overview (Fig.12). CSD is assessed by using a software (GHLab), (44). The data from color-DTI recordings of the LV/RV is imported to GHLab and processed by the Software. The software processes and adopts different parameters, such as, acceleration, velocity, and pattern recognition in order to create CSD (Fig13). CSD allows visualization of various cardiac mechanical events as a circular diagram. CSD displays several different parameters, such as tissue velocity, duration of time intervals, stroke lengths of the atrioventricular (AV)-piston, flow velocities, deformation information, and ECG. CSD represents a graphical view of these parameters of cardiac events. The diagram can be constructed with one outer circle (LV) or two outer circles corresponding to LV and RV demonstrating, the global timing of different time-events of cardiac cycle, where a complete circle corresponds to one cardiac cycle. The displacement of the AV-piston at the basal level of cardiac walls is displayed as a black circle in the middle of the diagram,

demonstrating information about the associated segments, strain, and strain rate. The beginning of the cardiac cycle corresponds to atrial contraction and the end with the slow filling. In this way the cardiac cycle is harmonize with the events in ECG signal activity, where normally the P-wave is the first activity seen in the ECG.

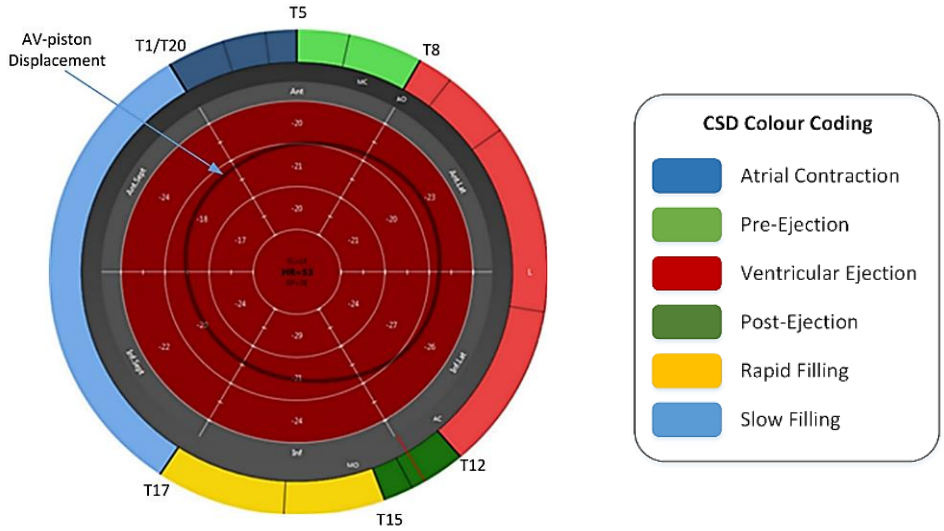

Figure 12 Cardiac state diagram. Outer circle represents duration of different cardiac time intervals of one cardiac cycle in one basal LV segment. The inner red circle shows strain information. The black circle indicates the displacement of the AV-piston in different segments at basal level of the LV. T1-T20 = Time marks during the cardiac cycle. (Reproduced with permission from Jonas Johnson)

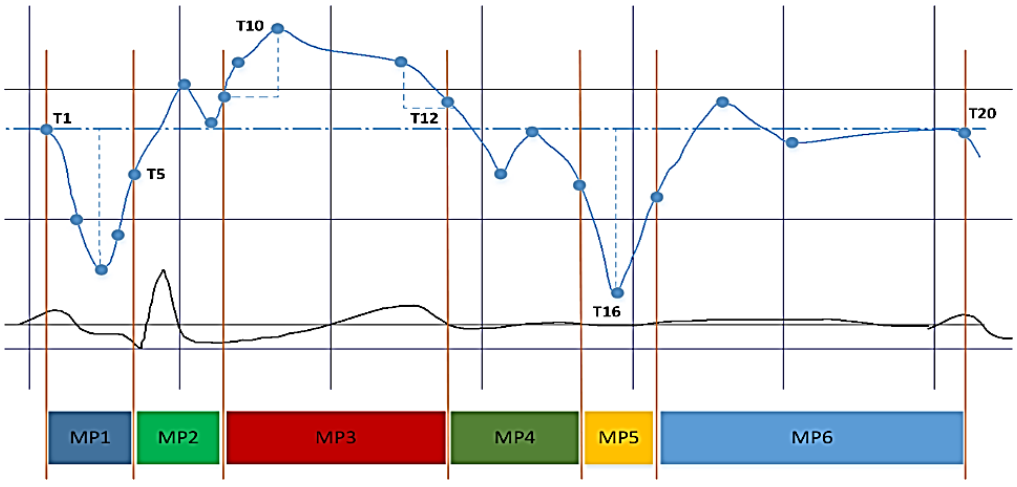

Figure 13. Illustration of velocity trace of different time events (T1-T20) of one cardiac cycle MPn = Main phase. The color coding corresponds to the same phases as the image above. (Reproduced with permission from Jonas Johnson)

1.4 RIGHT VENTRICLE

RV is located in the chest behind the sternum and anterior to the left ventricle (45) comprising mostly of a thin muscular layer wrapping around the left ventricle. In frontal plane, it is triangular-shaped and in cross-sectional plane, crescent-shaped. Anatomically it consists of 3 distinct parts: i) the inflow consisting of tricuspid valve apparatus, ii) apex, and iii) the outflow consisting of smooth muscle (46). Imaging of RV with 2D echocardiography is hampered owing to its location in the chest and its anatomical characteristics . Three-D echocardiography is overcoming many of the limitations of 2D echocardiography and is a promising modality in assessment of RV geometry and function.

1.4.1 Right ventricular size

Due to the anatomical complexity of the RV, using 2D echocardiography images from multiple acoustic windows should be acquired and measured in order to obtain an comprehensive assessment of RV size (9). Linear end-diastolic measurement of proximal- and distal right ventricular outflow tract (RVOT) in parasternal views and basal and mid-ventricular measurement of RV end-diastolic diameter in apical views have been recommended. In addition end-diastolic and end-systolic measurements of RV area in RV focused apical views by manually tracing the endocardial border has been recommended (9).

1.4.2 Right ventricular function

Complexity of RV anatomy renders difficulties in the assessment of RV function. Therefore, the latest guidelines recommend using a number of surrogate echocardiographic parameters in evaluation of RV function (9) Further, the majority of RV systolic parameters are load dependent (47).

1.4.3 Right ventricular ejection fraction

Assessment of right ventricular ejection fraction (RV EF) by 2D echocardiography has important limitations, and a number of studies report lack of accuracy (48). Although in comparison with cardiac magnetic resonance (CMR), 3DE underestimates RV volumes and EF, evaluation of RV EF using 3D echocardiography is recommended because it has been shown to be more accurate and reproducible (49). Since RV EF is reflecting an

integrated interaction between RV contractility and loading conditions, it cannot be considered a reliable parameter in quantifying RV systolic function in patients with pressure or volume overload. RV EF has been reported as an independent predictor of mortality in patients with heart failure (50).

1.4.4 Tricuspid annular plane systolic excursion

In systole, tricuspid annulus will normally descend 1.5-2.4 cm towards apex. This longitudinal motion of tricuspid annulus can be displayed using M-Mode echocardiography through lateral tricuspid annulus in apical four-chamber view. Accordingly, on the M-mode recordings the magnitude of the displacement of the lateral tricuspid annulus is measured and the tricuspid annular plane systolic excursion (TAPSE) is obtained. Strong correlation between TAPSE and parameters of global RV function as radionuclide-derived RV EF and CMRI-derived RV EF has been reported(51, 52). TAPSE is one-dimensional with the assumption that the regional, longitudinal displacement of the basal RV segment represents global RV function. Since it is a one-dimensional measurement relative to transducer it can over- or underestimate RV function due to overall heart motion (53). TAPSE is load dependent and the change in severity of functional tricuspid regurgitation (TR) may significantly affect its results. Previous studies have demonstrated association between TAPSE less than 1.5 cm and poor prognosis after acute myocardial infarction (54).

1.4.5 Tricuspid annular peak systolic velocity

Tricuspid lateral annular peak systolic velocity (RVS) is measured using color DTI or PW-DTI at the level of tricuspid lateral annulus with the curser parallel to the annulus. RVS is easy to obtain, reproducible and correlates well with other parameters of global RV function (55). Similar to TAPSE, RVS is a one-dimensional surrogate of RV function, measuring the velocity of longitudinal motion of RV free wall at basal segment relative to the position of the transducer. As such, it is influenced by the overall cardiac motion and can over- or underestimate RV function. Further, RVS is influenced by age and is reduced with increasing age (56). A number of studies have acknowledged a good correlation between TAPSE and RVS (55). RVS less than 9.5 is suggestive of RV dysfunction.

1.4.6 Fractional area change

Fractional area change (FAC) is a good measure of global RV performance, which is well-correlated with MRI-derived RV EF (57) and associated with outcomes in a variety of cardiovascular diseases (58, 59). In order to assess RV FAC, the RV endocardial border is traced manually and end-diastolic and end-systolic areas are obtained in RV-focused apical four-chamber view to calculate RV FAC (%) = 100 x (RV EDA - RV ESA)/RV EDA. While tracing, care must be taken to include trabeculations in the cavity and avoid apical foreshortening. Calculation of RV FAC requires good RV images with good endocardial delineation and as a measure of overall RV systolic function does not include RVOT (contributing to 25-30% of RV volume). RV FAC less than 35% indicates RV systolic dysfunction.

1.4.7 Right ventricular strain and strain rate

RV longitudinal strain is measured as the percentage of systolic, longitudinal shortening of RV free wall from base towards the apex, and RV strain rate is the rate of the shortening. RV longitudinal strain can be measured using either DTI or STE (60). Although, the correlation between the methods is moderate, both techniques have shown to be accurate and feasible in discriminating physiology from pathology (61). DTI-derived RV strain renders a number of limitations as: angle-dependency, large longitudinal motion of RV free wall requiring high frame rates, and influenced by age and heart rate. There are a number of issues in regard to measuring strain by STE. There are inconsistencies in measuring and reporting RV LS. While in some studies only 3 segments of RV free wall are included, in other studies an additional 3 segments of interventricular septum are also included. There are also inconsistencies in normative values, since the normal values are strongly intervendor-dependent. However, assessment of RV strain is evolving as robust and feasible in quantification of RV mechanical function as the body of evidence for its prognostic value in various cardiac disease (heart failure (62), AMI (63), amyloidosis (64), pulmonary hypertension (65)) is growing. The threshold of RV strain is set at -20% by the recent guidelines (9).

1.4.8 Right ventricular diastolic function

Assessment of RV diastolic function is not part of clinical evaluation of RV function. While there is a body of evidence on diagnostic and prognostic implications of RV systolic dysfunction, there are only a few studies addressing the prognostic implications of RV diastolic dysfunction (66).

1.4.9 Right ventricular index of myocardial performance

As previously described, RIMP is an estimate of global RV performance combining systolic and diastolic time intervals of cardiac cycle. Several techniques for assessment of RIMP are available. However, pulsed spectral Doppler (PW) of the tricuspid inflow and RV outflow, and DTI of the lateral tricuspid annulus are the most common methods. In patients with significant arrhythmias, using pulsed Doppler for calculation of is not recommended given the significant RR variation in inconsecutive cardiac cycles. This limitation is overcome in calculating RIMP by DTI since a single RR-interval is used. RIMP >0.43 by PW Doppler and >0.54 by DTI indicates overall RV dysfunction.

1.5 IMPACT OF ISCHEMIA AND REVASCULARIZATION ON MYOCARDIAL FUNCTION

The tight association between coronary blood flow supply, myocardial oxygen demand, and contractile performance of cardiac myocytes is the fundamental principle of cardiac physiology. Further, a close coupling between regional coronary blood flow and state of contractile function of cardiac myocytes, known as perfusion-contraction matching, has been demonstrated. It is known that reduced coronary blood flow results in decreased myocardial contractile function. Depending on the severity and duration of flow reduction, decreased contractile function might be reversible or permanent. When the coronary blood flow i severely reduced, and persists for more than 20 minutes, the contractile function of the myocardium may irreversibly be damaged due to development of necrosis. However, when myocardial ischemia is brief or moderate myocardium remains viable and the contractile dysfunction can be reversed upon reperfusion/revascularization. This condition of chronic adaptive reversible reduction in contractile function is known as myocardial hibernation. However, contractile recovery may require considerable time despite restoration of adequate coronary blood flow supply. This condition of flow-function mismatching is known as myocardial stunning. On the other hand, if the myocardial contractile dysfunction is due to fibrosis then no recovery after revascularization therapy is to be expected.

Several imaging modalities including DSE are commonly used in the assessment of myocardial viability, and have the ability to predict recovery of function after revascularization.

1.6 BNP

B-type natriuretic peptide (BNP) was first identified in brain extracts, thus it is also known as Brain natriuretic peptide. BNP is secreted from ventricular myocardium in response to an increase in wall stress pressure or volume-overload (67). After synthesis BNP is cleaved to proBNP. When in the circulation, proBNP is cleaved into the active portion of BNP and inactive amino-terminal NT-proBNP. The half-time of BNP is 20 min whereas the half life of NT-proBNP is 120 min (68). BNP and NT-proBNP are expressed in pg/ml or µmol/L. The conversion factor of BNP is 1pg/ml= 0.289 µmol/L, and the conversion factor for NT-proBNP is 1pg/ml= 0.118 µmol/L (68). The physiological effects of BNP are many and include peripheral vasodilatation, as well as inhibition of renin-angiotensin-aldosterone system (68). Cardiac conditions such as (AF; pulmonary embolism) or some non-cardiac conditions such as (renal impairment) will result in increased circulatory BNP-levels due to increased volume or pressure overload on cardiac chambers. BNP levels increase with age and are likely to reduce in obese patients (69). It has been demonstrated that BNP and NT-proBNP have similar diagnostic performance in patients with heart failure, patients with asymptomatic left ventricular dysfunction and in patients with renal failure. BNP and NT-proBNP are used as powerful diagnostic markers in the management of patients presenting with heart failure symptoms and can be used as a complementary method to guide therapy in heart failure (70). According to recent ESC guidelines, heart failure is unlikely if BNP<35 pg/ml or NT-proBNP<125 pg/ml . Similarly, in patients with suspected acute heart failure the diagnosis is unlikely if BNP<100 pg/ml and/or NT-proBNP<300 pg/ml (71).

Further, several studies suggest that BNP and NT-proBNP are valuable prognostic markers of death and cardiovascular events in patients with heart failure, CAD and valvular heart disease (72-74).

In conclusion, both BNP and NT-proBNP are valuable diagnostic and prognostic biomarkers reflecting increased myocardial wall stress independent of underlying specific pathology. Thus, they reflect cardiac disease in general and not a specific pathology.

2 AIMS

STUDY I

In patients with coronary artery disease (CAD), the goal of surgery is to relieve ischemia and to improve myocardial function. We sought to evaluate the effects of CABG on LV function in patients with established ischemic heart disease. In addition to other conventional methods we addressed an objective measurement of cardiac performance after CABG by using time intervals in MPI assessed by PW-DTI of four different sites around the basal portion of the LV.

STUDY II

In this study, we aim to characterize the impact of CABG on RV function in patients with advanced CAD undergoing isolated CABG. The impact of CABG on RV function was assessed using conventional parameters as TAPSE and RVS as compared to RIMP as an estimate of global RV performance. Further, the effect of CABG on RV function during DSE was evaluated.

STUDY III

This is predefined post hoc analysis of a single-center randomized trial. We seek to compare changes in both load dependent and independent metrics of RV performance in patients treated with full sternotomy AVR vs. MIAVR. In this study, we aimed to study alterations in RV longitudinal function, RV global function, and RV contractility following AVR vs MIAVR.

STUDY IV

In this study, we evaluate the independent role of postoperative BNP, assessed in a stable clinical setting 3 months after CABG for predicting long-term outcomes following isolated, primary CABG. Further, in a subpopulation of patients we evaluated the correlation between LV-MPI, RIMP, and BNP respectively as markers of myocardial function.

3 MATERIALS AND METHODS

3.1 PATIENT POPULATION (STUDY I, II & IV)

From May1995 to February 2001, 746 patients were admitted to the hospital due to angina and were assigned to CABG based on findings on coronary angiography and according to existing guidelines. Patients with (i) atrial fibrillation; (ii) severe valvular heart disease; (iii) pacemaker; (iv) recent myocardial infarction (within 4 weeks); and (v) previous CABG were excluded. This left, 99 patients to be included in the study. All the included patients underwent blood tests, Bicycle exercise test, comprehensive echocardiography, and Dobutamine stress echocardiography at the time of initial angiography (Fig 14). In a subpopulation of 46 patients, Doppler Tissue Imaging (DTI) echocardiography was also performed (Table 3). Postoperative clinical follow-up was performed 3 months after CABG. At that point all the tests which were performed upon inclusion, including a follow-up angiography, were performed again at follow-up. In the patients with DTI, LV-MPI and RIMP were assessed respectively at rest and at peak DSE both before CABG and after CABG. Generally speaking high values of LV-MPI/RIMP indicate myocardial dysfunction, while low values indicate good myocardial performance.

The patients were followed-up by send-out questionnaires and additionally through medical records for a median of 5 years (3-7 years) after receiving CABG (Fig.14).

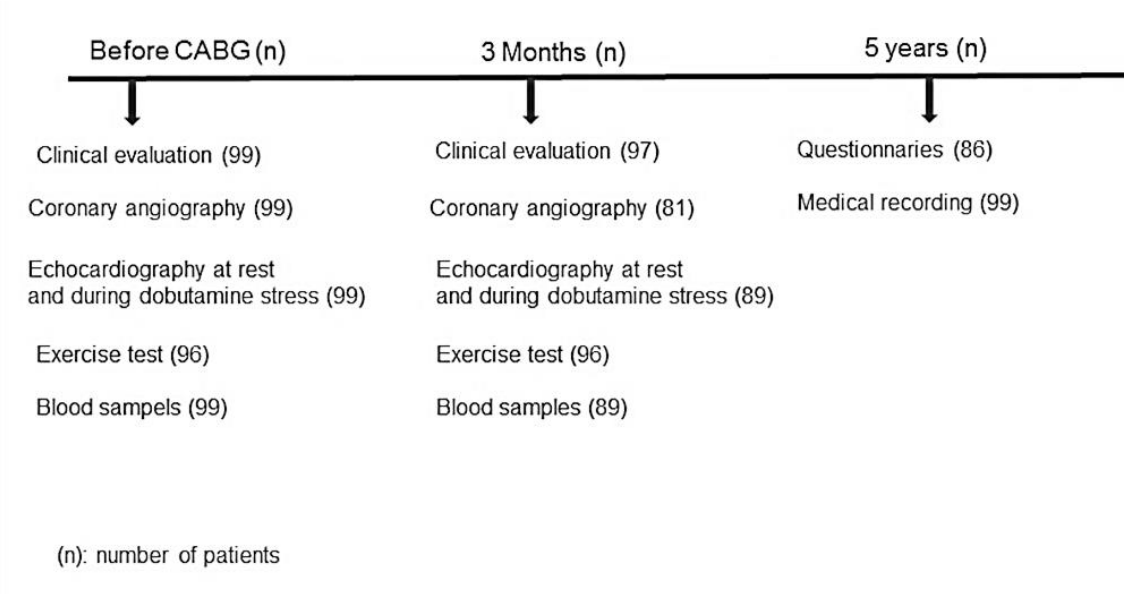

Figure 14. Chart flow of studies (1, II, IV) showing the number of patients evaluated in each setting, before CABG, 3 months after, and 5 years after CABG. CABG: coronary artery bypass grafting.

3.2 ECHOCARDIOGRAPHY (STUDY I, II & IV)

Echocardiography examination was performed with patients lying on their left lateral side and using a Sonos 5500 (Hewlett-Packard, Andover, MA, USA). A complete 2-D and Doppler examination was performed.

3.2.1 Measurement of cardiac chamber Size

From the parasternal long axis view, linear internal dimensions of the LV were measured at end-diastole (LVEDD) and end-systole (LVESD). LV volumes were obtained from apical four- and two-chamber view, at end-diastole (LVEDV) and end-systole (LVESV) using Simpson's biplane.

Basal RV linear dimension (RVD1) was measured as the maximal transversal dimension in the basal one-third of RV inflow at end-diastole. Proximal RV outflow (RVOT prox) was obtained in parasternal long-axis view and measured at end-diastole from the anterior RV wall to the interventricular septal-aortic junction.

3.2.2 Left ventricular ejection Fraction

LV systolic function was quantified by ejection fraction (LVEF) using Simpson's biplane method from apical four- and two-chamber views: LVEF (%)= 100 x (LV EDV-LV ESV)/LV EDV.

3.2.3 Left ventricular diastolic function

From apical four-chamber view, PW-Doppler of mitral inflow was obtained. Then mitral peak early (E), and late inflow velocity (A) were measured and mitral E/A ratio was calculated. Peak early systolic tissue velocity of the septal wall at the level of mitral annulus was measured using PW-DTI Accordingly, the ratio of E/E´ was calculated.

3.2.4 Right ventricular systolic function

M-mode recordings of RV free wall at the level of tricuspid annulus were obtained and TAPSE was measured as the maximum of displacement of the RV lateral annulus (Fig. 15). RVS was measured as the peak systolic velocity of lateral tricuspid annulus using PW-DTI.

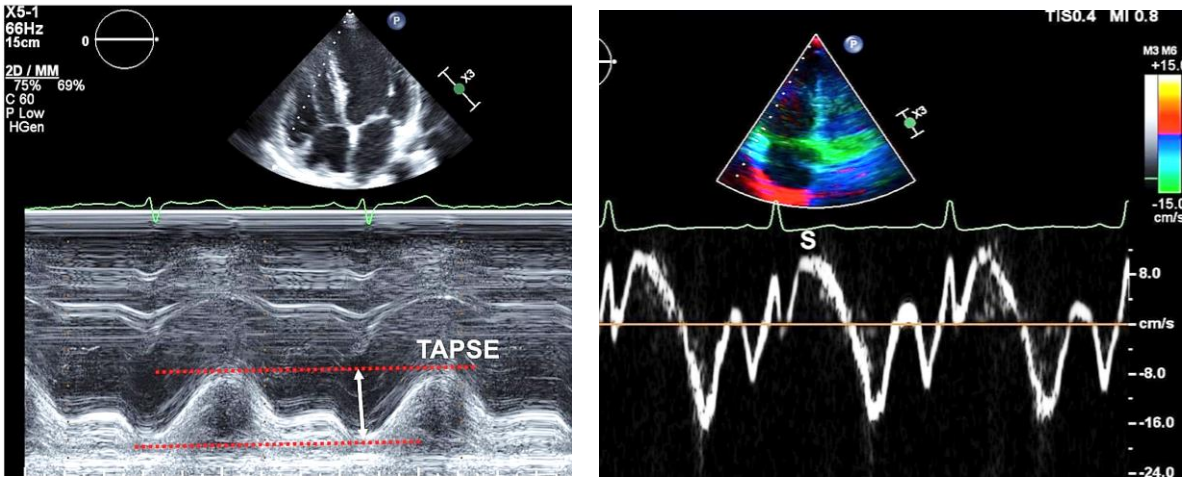

Figure 15. Assessment of tricuspid annular systolic excursion (TAPSE) by M-mode (Left), and measurement of right ventricular peak systolic velocity (RVS) using pulsed Doppler tissue imaging.

3.2.5 Right ventricular diastolic function

Diastolic RV function was quantified by calculating the tricuspid E/A ratio. From apical four-chamber view, PW-Doppler of tricuspid inflow was obtained, and tricuspid peak early inflow velocity (E), tricuspid peak late inflow velocity (A) was measured and subsequently tricuspid E/A ratio was calculated.

3.2.6 Cardiac time intervals and myocardial performance index by pulsed Doppler tissue imaging

Cardiac time intervals were assessed using PW-DTI recordings which were obtained online using a variable frequency phased array transducer (2.0-4.0 MHz), a low filter wall setting (50 Hz), and a small sample volume of 1.7 mm. Accordingly, the gain was optimized. PW-DTI images of the septal, lateral, inferior, and anterior walls of the LV and RV free wall were obtained at the level of mitral annulus and at the level of lateral tricuspid annulus from apical 4-chamber view respectively. The subsequent analyses were performed from the digitally stored PW-DTI recordings. The time interval between

cessation (A´) and the beginning of the (E´) was measured as the total combined duration of (ICT + ET + IVRT). The ET was measured as time interval between onset and cessation of the S-wave. MPI was calculated as (ICT + ET + IVRT) – ET / ET . Global LV MPI was calculated as an average of MPI from those LV sites as mentioned above. Accordingly, RIMP was calculated by the same way at the lateral tricuspid annulus.

3.2.7 Dobutamine stress echocardiography

DSE was performed using a standard protocol at the Echo-lab. Briefly, the dobutamine infusion started at a starting dose of 5 μg/kg/min and was increased every 3 minutes up to a maximum dose of 40 μg/kg/min. If required, intravenous atropine sulfate up to 1 mg was also in addition administered. The test was terminated whenever the endpoints were reached as recommended by the European Association of Echocardiography (75).

WMSI was calculated using a 16-segment model. Segmental wall motion score was defined as follows: 1=normal/hyperkinetic; 2=hypokinetic; 3=akinetic; 4=dyskinetic; 5=aneurysm. The WMSI was calculated as the sum of scores divided by the number of segments visualized. An ischemic response was defined as development of new wall motion abnormality in at least 2 adjacent segments of LV wall.

3.3 CORONARY ANGIOGRAPHY

Coronary angiography was performed using the standard protocol of the angiography lab. All angiographic images was interpreted by an experienced interventional cardiologist. Any stenosis of ≥ 50% in coronary arteries or their major branches was considered significant.

3.4 BICYCLE EXERCISE STRESS TEST

Upright bicycle exercise stress tests were completed using a stationary bicycle and the 10-point Borg scale (76). Conventional clinical and ECG monitoring was used during the test. The peak heart rate, systolic blood pressure, respiration, symptoms and estimated work load were recorded for each test.. The test was ended using endpoints recommended at the lab(77) The work load was measured as watts.

3.5 BNP

Blood samples were obtained from antecubital vein using vacutainer equipment and without implying stasis. The samples were prepared immediately. The plasma samples were stored at -80 C for future analysis. The BNP was measured using immuno radiometric assay (IRMA). In this method, two monoclonal antibodies react against two sterically distinct portions of the BNP molecule. The first is "coated" on a bead, while the other is tagged with 125 [I] and used as a tracer. The BNP molecule present in the sample is bound between the two antibodies and thus anchored to the antibody associated with the bead. Unbound tracer is eliminated in the following washing steps, and the bead only retains the antibody / antigen / tracer complex. The amount of radioactivity bound to the solid phase is proportional to the amount of BNP present in the sample.

3.6 PATIENT POPULATION (STUDY III)

The CMILE (Cardiac Function after Minimally Invasive Aortic Valve Implantation) study was designed as a randomized, single-center, open label study. Adult patients assigned to surgical aortic valve replacement at Karolinska University Hospital in Stockholm, Sweden were eligible for inclusion into the study. Patients were included in the study between October 2013 and July 2015. Patients were excluded if they had (i) reduced left ventricular Ejection Fraction (LVEF) <45%); (ii) previous cardiac surgery; (iii) concomitant other severe valvular heart disease; (iv) coronary artery disease (CAD) requiring surgical intervention; and/or (v) urgent or emergency surgery (Fig. 16). Coronary angiography for evaluating coexisting CAD was performed prior to surgery. Echocardiography was performed within one week before surgery and 40 days post-surgery.

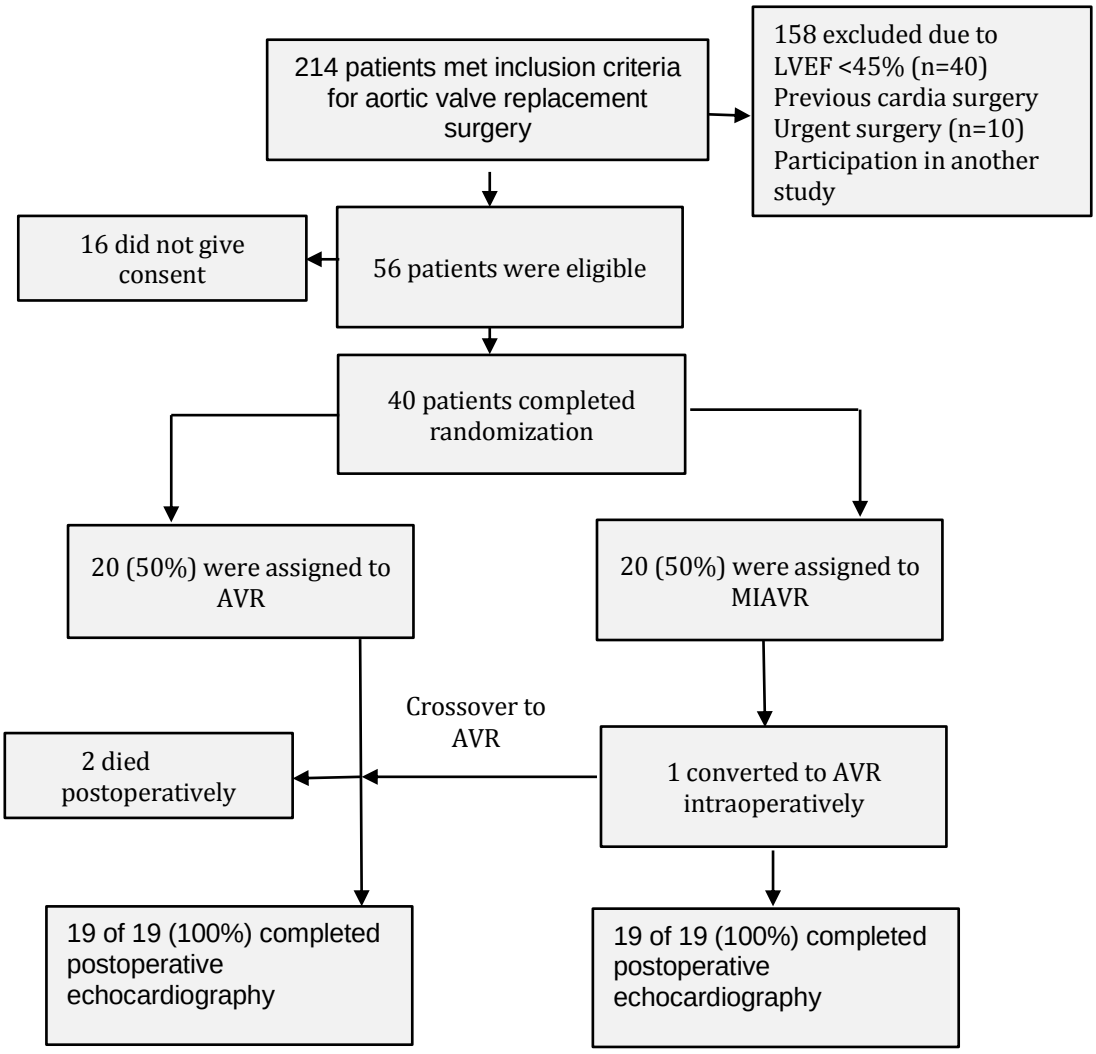

Figure 16. Chart flow of patients in study III, AVR: aortic valve replacement surgery, MIAVR: minimally invasive aortic valve replacement surgery.

3.7 SURGICAL TECHNIQUES (STUDY III)

3.7.1 Minimally invasive aortic valve replacement surgery (MIAVR)

MIAVR was performed via a J-shaped upper partial ministernotomy approach. A skin incision of approximately 6 cm in the midline over the upper part of the sternum was performed (Fig 17). A partial J-shaped skin incision was extended into the third intercostal space. A small vertical pericardial incision anterior to ascending aorta was performed, and subsequently the aortic valve was exposed. Cardiopulmonary bypass with central arterial and central or peripheral venous cannula was established. Subsequently, antegrade custodial cardioplegia solution was administered. CE marked mechanical or bioprosthetic aortic valves were implanted. The bioprosthetic valves could be conventional stented, or sutureless bioprostheses. The pericardial incision was closed at the end of procedure.

3.7.2 Conventional full sternotomy aortic valve replacement surgery (AVR)

The heart was exposed through full median sternotomy (Fig 17). A complete pericardial incision was performed. Cardiopulmonary bypass was established. Antegrade and/or retrograde cold blood cardioplegia was administered. CE marked mechanical or bioprosthetic aortic valves were implanted. The pericardial incision was not closed at the end of procedure.

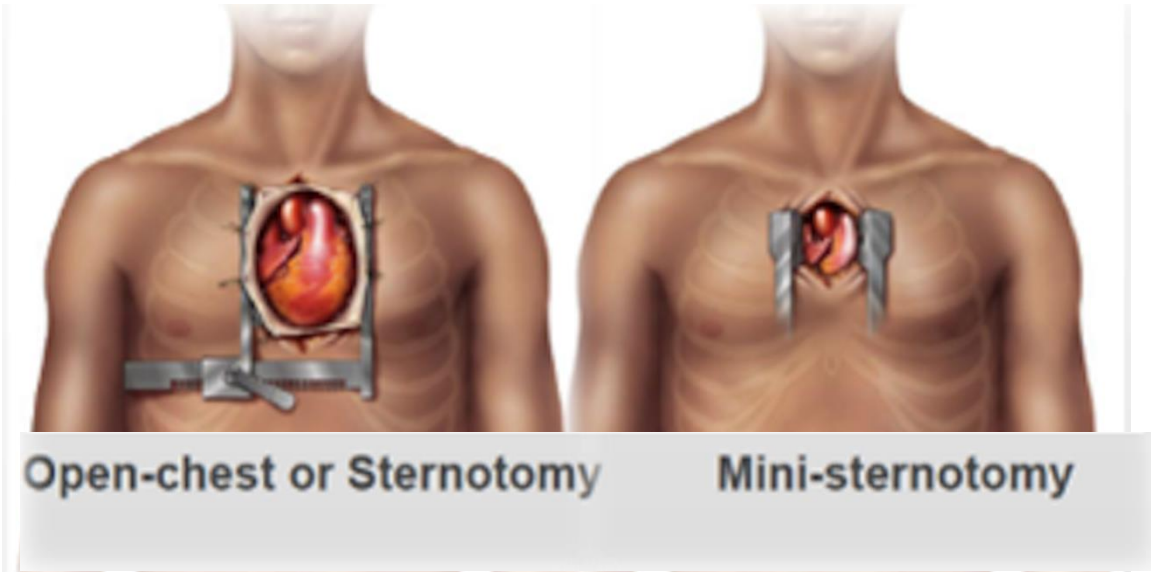

Figure 17. Illustration of Edwards showing conventional aortic valve replacement surgery (AVR), (left) and minimally invasive aortic valve surgery (MIAVR), (right).

3.8 ECHOCARDIOGRAPHIC MEASUREMENTS (STUDY III)

All echocardiography examinations were performed on a Vivid E9 (GE, Healthcare, Horten, Norway). The images were digitally stored. All subsequent analyses were performed off-line on an EchoPAC station , version 201 (GE Vingmed Ultrasound AS, Horten, Norway). All linear measurements and LVEF were assessed as previously described.

3.8.1 Left ventricular global longitudinal strain

Speckle tracking Echocardiography was applied to assess LV-GLS and LV-GLSR. The image quality and the gain setting was optimized. The depth of cine loops were adjusted in order to achieve a minimum frame rate 50/s. Off-line analysis was conducted with dedicated, commercially available software for speckle tacking 2D-strain analysis on the EchoPAC (GE, version 201, US). LV GLS was measured in three standard apical LV views and averaged. Measurements started in the apical long axis view, then apical four-chamber view and ended with apical two-chamber view. An automatic estimate of aortic valve closure was used by the software to predefine end systole. The software used an ECG-Derived time marker for defining end systole which was set as the end of T-wave on ECG. The software automatically calculated segmental strain and GLS (Fig 18).

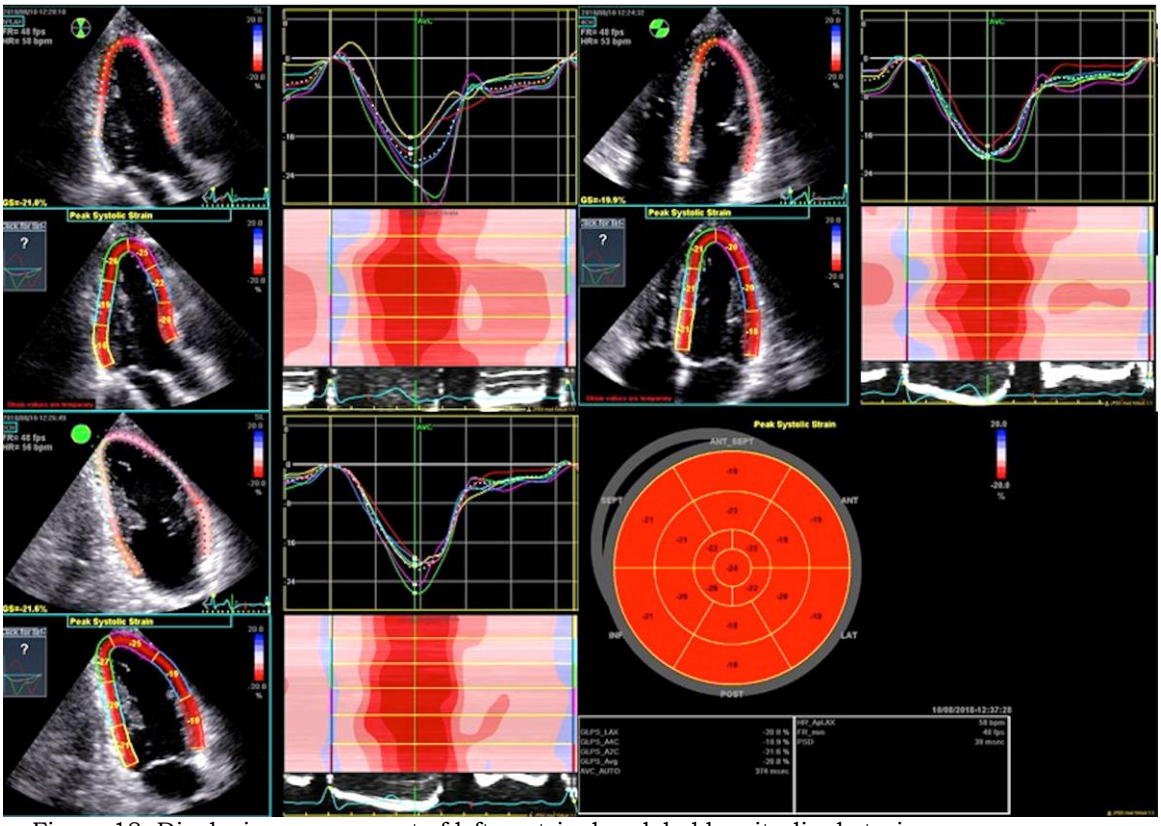

Figure 18. Displaying assessment of left ventricular global longitudinal strain.

3.8.2 Right ventricular longitudinal function

TAPSE was obtained as previously described. RVS was assessed using GHLab (Gripping Heart AB, Stockholm) software (43) and measured as the maximal myocardial velocity during right ventricular ejection (Fig. 19).

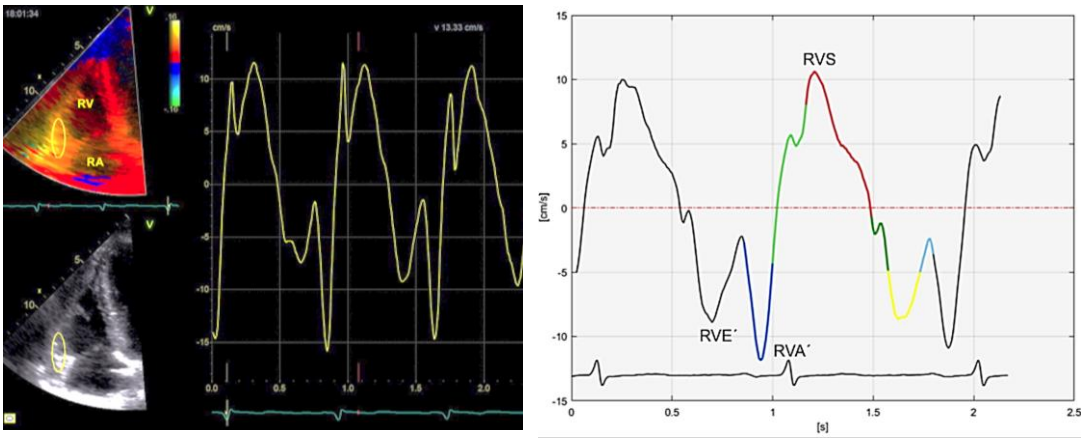

Figure 19. Position of ROI on color-DTI echocardiogram (left), measuring RVS by CHLab (right).

3.8.3 Fractional area change

RV endocardial border was traced manually at end-systole and at end-diastole. The tracings were applied manually from the lateral tricuspid annulus along the RV free wall to the apex and along the interventricular septum back to the medial tricuspid annulus. Trabeculations, papillary muscles and moderator band were included in the RV cavity area. RV FAC (%) was calculated: 100 x (EDA-ESA)/EDA (Fig.20).

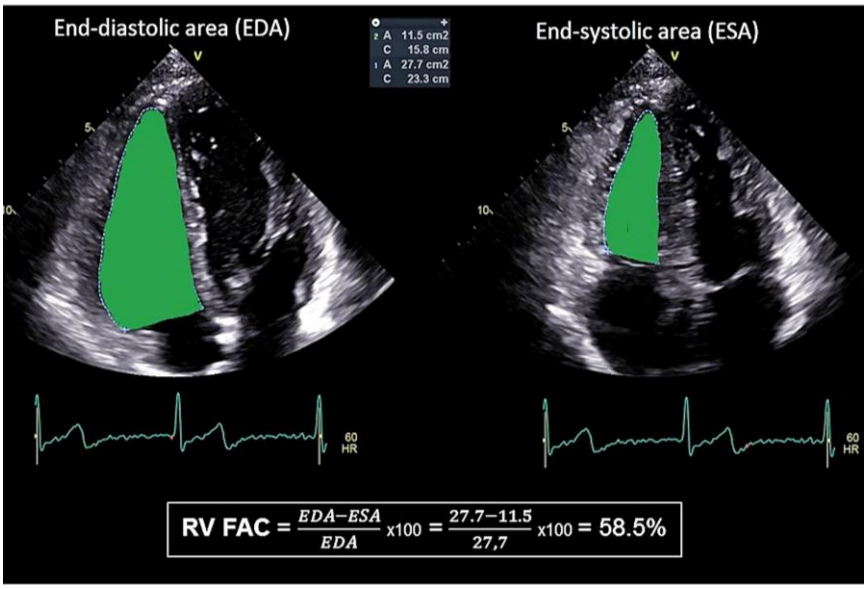

Figure 20. Assessment of right ventricular (RV) fractional area change (FAC) by 2D echocardiography.

3.8.4 RV longitudinal strain and Strain rate

Speckle tracking Echocardiography was applied on RV-focused four-chamber view to assess RV-LS and RV-LSR. The depth of cine loops was adjusted in order to achieve a minimum frame rate 50/s. The gain setting was optimized. Off-line analysis of the RV apical four-chamber view was conducted with dedicated, commercially available software for speckle tacking 2D-strain analysis on the EchoPAC (GE, version 201, US). The endocardial border of the RV free wall was marked and the size of the ROI was adjusted in order to limit it to the myocardium. The tracings were manually corrected whenever needed. The RV free wall was divided into three segments: basal, mid, and apical. The software automatically calculated segmental and global RV-LS and global RV-LSR through out cardiac cycle (Fig. 21).

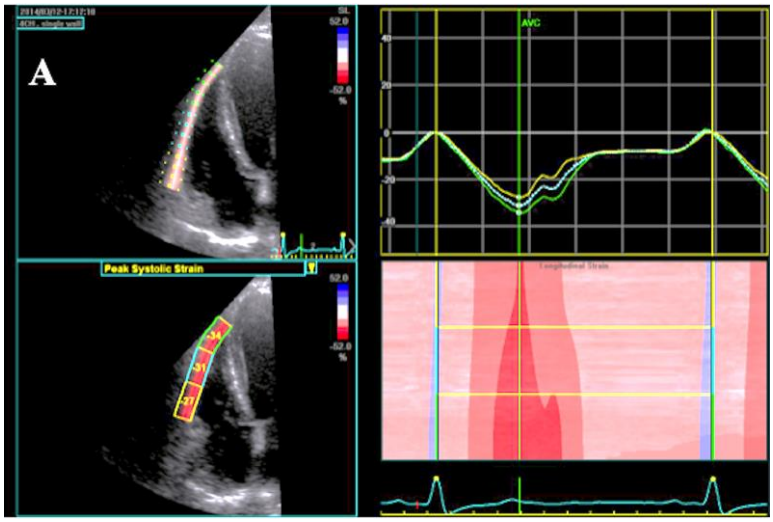

Figure 21 Assessment of right ventricular strain (A) and strain rate (B).

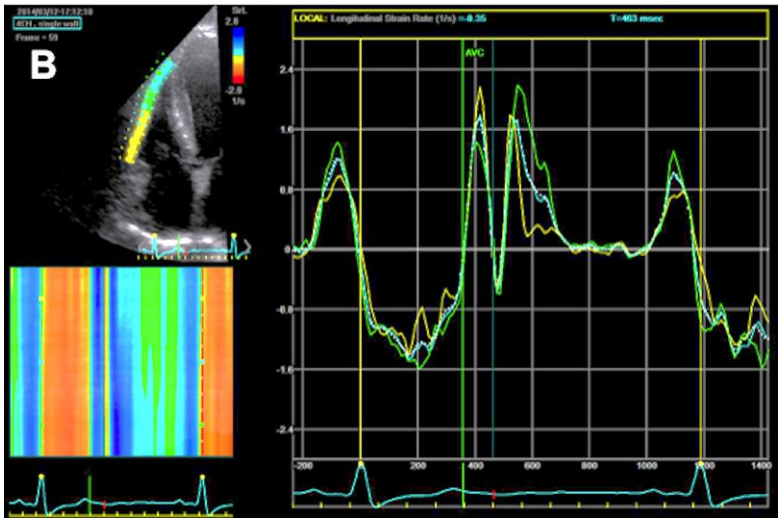

3.8.5 Cardiac time intervals and myocardial performance index by GHLab

The traces of myocardial longitudinal motion from the Tissue Doppler Imaging (TDI) recordings were imported to software called GHLab (Gripping Heart AB, Stockholm, Sweden), (78), where the software automatically identified the different phases of the cardiac cycle and myocardial velocities. The software identified the different mechanical cardiac time events using the Dynamic Adaptive Piston Pump (DAPP) principle that describes the heart as a mechanical pump controlled by its inflow . In this model, the movement of the atrioventricular-plane initiates the mechanical functioning of the heart, thus the atrial contraction is considered to be the starting point of the cardiac cycle. The different phases in the cardiac cycle are defined by shifts in the myocardial mechanical work rather than by the opening or closure of the cardiac valves. The terms pre-and post-ejection are used instead of isovolumic contraction and relaxation. ROI is chosen at the level of mitral annulus at six different locations of the LV which are: anterior septal, anterior, anterior lateral, inferior lateral, inferior, inferior septal, and inferior and accordingly the at the level of tricuspid annulus of RV free wall The six phases of the cardiac mechanical events in one cardiac cycle were manually identified as: atrial contraction, pre-ejection period (PEP), ventricular ejection time (ET), post-ejection period (POP), rapid filling/early diastole, and slow filling/diastasis (Fig 22). The software measured the duration of each phase. Subsequently, myocardial performance index of the left and right ventricles (LVMPI, RIMP) were obtained as follows PEP + POP/ET. Peak myocardial velocity during ventricular ejection (S), early diastolic velocity (E´) and late diastolic velocity (A´) were obtained from the software (Figure 19). Then ratio of E´/A´ was calculated.

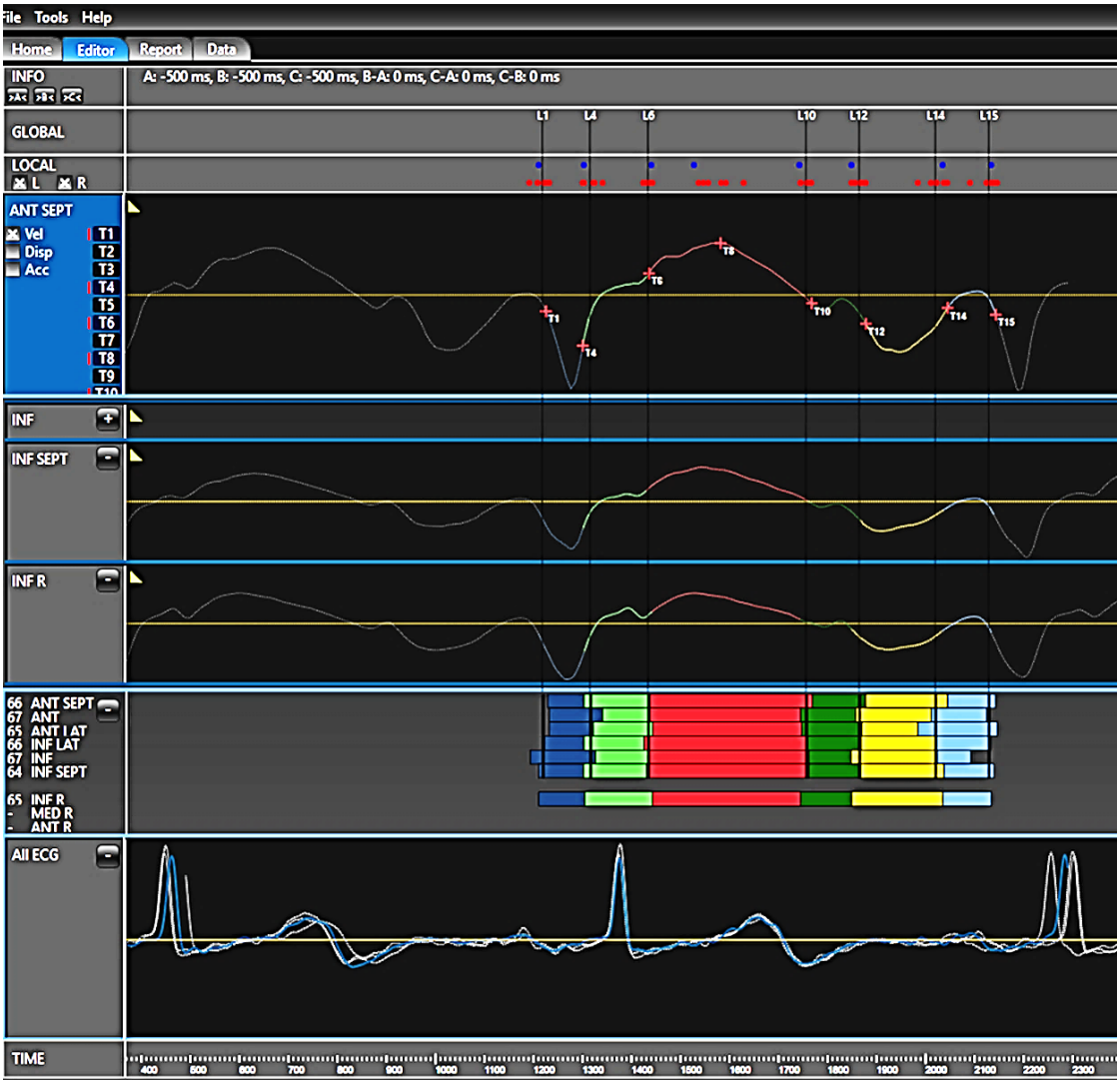

Figure 22.Image of data processing in GHLab.

3.9 STATISTICS

Data was analyzed using commercially available statistical software (SPSS version 16 and version 22, IBM Corporation, Armonk, NY, USA)). In addition, MATLAB was used in study III. Normal distribution of continuous data was tested by visual inspection of histograms assessing normality. In addition, normality was assessed using Shapiro-Wilks test. Normally distributed, continuous data are reported as means ± SD. Non-normally distributed, continuous variables are reported as medians and quartiles. Categorical data are presented as frequencies and percentages.

Normally distributed, paired data were compared using students paired t-test. Wilcoxon's signed-rank test was used to compare paired data that were not normally distributed. Fisher exact test or Chi-square was used to compare proportions. Non-parametric data were analyzed using Mann-Whitney.

In study IV, empiric receiver operating characteristic (ROC) curve was used to determine the cut-off value of the BNP in predicting death and major adverse outcomes (MACES). The level of significance for predicting MACE was determined using BNP, Clinical- and echocardiographic variables in a univariate regression model, in order to assess the independent association of variables with postoperative MACE. The variables in the univariate regression model that were statistically significant were entered into a multi regression model. Unadjusted odds ratio (OR) with 95% confidence interval (CI) was assessed using univariate logistic regression and adjusted OR with 95% CI was computed using multivariate regression analysis.

3.10 ETHICS

The study was conducted in adherence to Declaration of Helsinki. Written informed consent was obtained from all participants in all studies. Local or regional Ethical committees approved the studies.

4 RESULTS

Tables 1 and 2 show clinical characteristics and medical therapy of the DTI-cohort in (study I, II & IV).

Table 1. Baseline clinical characteristics (n=46), studies (I,II & IV)

Parameters	Result
Female/male gender [n (%)]	9 (19.6) / 37 (80.4)
Age [years, mean (SD)]	64.3 (9.6)
Systolic blood pressure [mmHg, mean (SD)]	148.6 (21.2)
Diastolic blood pressure [mmHg, mean (SD)]	84.3 (10.5)
Body mass index [Kg/m2, mean (SD)]	26.7 (3.1)
Creatinine [µmole/L, mean (SD)]	97.0 (21.2)
Hypertension [n (%)]	22 (47.8%)
Hyperlipidemia [n (%)]	43 (93.5%)
Diabetes [n (%)]	10 (21.7%)
Smoker [n (%)]	9 (19.6%)
Previous MI [n (%)]	20 (43.5%)
CCS class [n (%)]	
I	5 (10.9%)
II	29 (63.0%)
III	11 (23.9%)
IV	1 (2.2%)
Coronary angiography [n (%)]	
One-vessel disease	1 (2.2)
Two-vessel disease	7 (15.2)
Multi vessel disease	38 (82.6)

n (%): number of patients with percentages in parentheses; SD: Standard deviation; MI: myocardial infarction; CCS: Canadian Cardiovascular Society.

Table 2. Medical therapy before CABG and 3 months after CABG (n=46), Study (I, II & IV)

Variable	Before CABG n (%)	After CABG n (%)	P-value
Beta-blocker	40 (87.0)	39 (86.7)	1.00
Calcium channel inhibitor	13 (28.3)	4 (8.9)	0.039
Long acting nitrates	30 (65.2)	1 (2.2)	<0.001
Diuretics	9 (19.6)	8 (17.8)	1.00
ACE-I/ARB	12 (26.1)	16 (35.6)	0.388
Statins	40 (87.0)	43 (95.6)	0.125
Digoxin	1 (2.2)	1 (2.2)	0.831
Insulin	5 (10.9)	4 (8.9)	1.00
Oral glucose-lowering agents	3 (6.5)	4 (8.9)	1.00
ASA	45 (97.8)	42 (93.3)	0.625

n (%): number of patients with percentages in parentheses; CABG: Coronary artery bypass grafting; ACE-I: Angiotensin-converting enzyme inhibitor; ARB: Angiotensin receptor blocker; ASA: Acetyl salicylic acid

4.1 STUDY I

Thirty six patients were included in the study. Only 6 patients (16.67%) were females. Previous myocardial infarction (MI) was present in 18 patients (50%). Angiography prior to CABG showed 3-vessel disease in the majority of patients (80%), .Except for Nitrates, patients were treated with same medical therapy following CABG as compared to before CABG. Before CABG 20 patients (56%) were treated with Nitrates. While, only 1 patient (2.8%) was treated with Nitrates following CABG .

4.1.1 Impact of CABG on LV function

Ejection fraction (EF) was mildly reduced at rest before CABG and it did not improve when values from pre-CABG was compared to post-CABG (42 ± 8% vs 43.7 ± 8%, P=0.4). However, EF improved during DSE comparing values from pre- to post-CABG (49.2 ± 9% vs 54.2 ± 9%, P= 0.01), (Table 3). Prior to CABG an ischemic response was observed in the majority of patients (34 (94.4%)) during DSE while, after CABG an ischemic response was seen only in 2 patients (2 (5.6%); P<0.0001). Similarly, WMSI improved significantly following CABG (1.40 vs 1.08, P<0.001).

Table 3. Echocardiographic measurements of the left ventricular function at rest and peak DSE, before and after CABG

Echocardiographic parameters	Rest pre-CABG	Rest post-CABG	DSE pre-CABG	DSE post-CABG
LV (ICT+IVRT) (msec)	177.0 (36)	135.3 (18)***	150.0 (31)	107.6 (22)***
LV -ET (msec)	341.0 (31)	307.9 (30)*	194.2 (35)	197.7 (29)
LV-MPI	0.61 (0.13)	0.45 (0.08)***	0.78 (16)	0.56 (0.1)***
EF (%)	42.7 (8)	43.7 (8)	49.2 (9)	54.2 (99)**
LV S (cm/sec)	6.4 (1.4)	6.4 (1.3)	8.9 (2.3)	9.0 (2.8)
LV E´ (cm/sec)	7.5 (2)	7.9 (1.8)	8.3 (1.9)	9.7 (3.0)*
LV A´(cm/sec)	8.4 (2)	7.7 (2.6)	11.6 (3.2)	10.7 (4.6)
Mitral E (m/s)	0.66 (0.17)	0.69 (0.19)	0.61 (0.21)	0.78 (0.20)**
Mitral A (m/s)	0.68 (0.19)	0.58 (0.20)**	0.83 (0.20)	0.85 (0.23)
Mitral E/A ratio	1.1 (0.51)	1.37 (0.71)**	0.74 (0.32)	0.94 (0.35)**
LV E/E' ratio	9.3 (3.1)	9.1 (2.8)	7.6 (2.6)	8.5 (2.4)
Heart rate (beats/min)	58 (10)	63 (10)* *	127 (14)	130 (18)

Data is represented as mean (SD). CABG: Coronary artery bypass grafting; DSE: Dobutamine stress echocardiography; ICT: Isovolumic contraction time, IVRT: isovolumic relaxation time; ET: Ejection time; MPI: myocardial performance index; EF: ejection fraction; LV: Left ventricular; S: peak annular longitudinal tissue velocity; E' (early) and A' (late): peak annular longitudinal tissue velocity; E: peak early inflow velocity; A: peak late inflow velocity.
Paired t-test: pre-CABG vs post-CABG.

* P < 0.05.

**. P < 0.01.

*** P < 0.001.

Global LV function assessed by LVMPI improved at rest when comparing values from pre-CABG to post CABG (0.60 ± 0.13 vs 0.45 ± 0.08, P<0.001), (Table 3). Accordingly, compared to pre- CABG LVMPI improved at peak DSE after CABG (0.78 ± 0.16 vs 0.56 ± 0.1, P<0.001), (Fig. 23). Accordingly, the improvement was consistent when LVMPI was adjusted for heart rate (P<0.001).

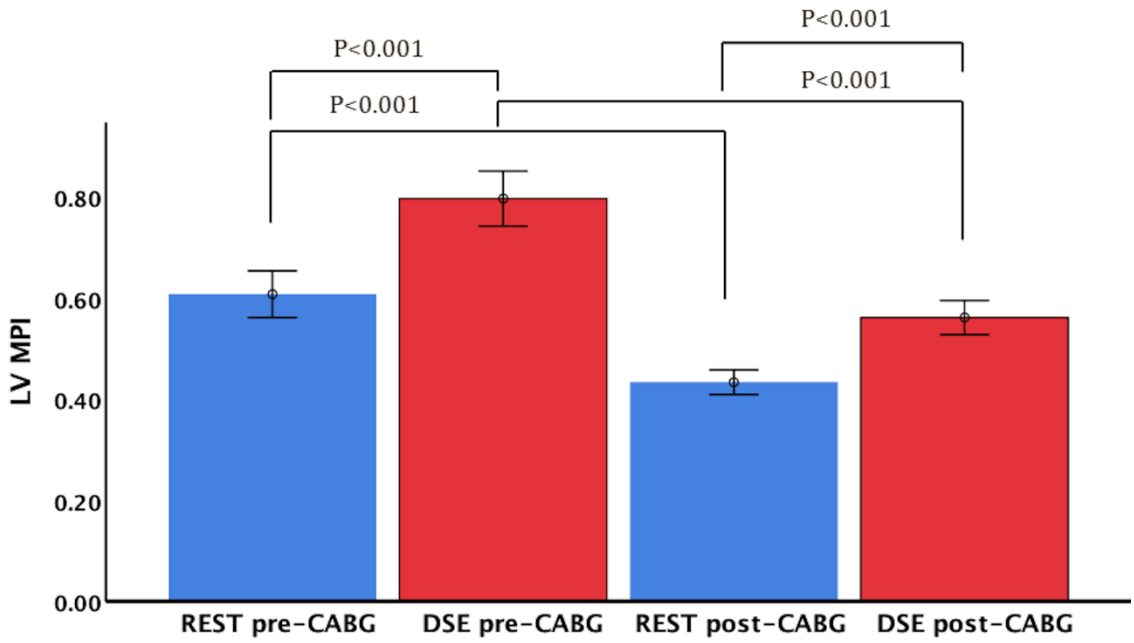

Figure 23. Alterations in LV-MPI from rest to peak DSE before and after CABG. LV: left ventricular, MPI: Myocardial performance index; CABG: Coronary artery bypass grafting; DSE dobutamine stress echocardiography.

4.2 STUDY II

Forty-two patients were included in the study. Mean age was (64 ± 9) years; 8 (19.0%) patients were female. Nineteen (45.2%) patients had hypertension, 9 (21.4%) had diabetes and 18 (42.9%) had a history of previous MI. Thirty-five patients (83.3%) had 3-vessel disease, whereas 37 (88.09%) had significant right coronary artery (RCA) stenosis. Conventional cardiopulmonary bypass was used in all patients undergoing CABG. Following CABG, open grafts were seen in 34 (80.9%) patients at follow-up angiography 3 months after CABG.

4.2.1 Impact of CABG on right ventricular function

Prior to CABG, RV systolic function as assessed by TAPSE (23.9 ± 4.5) and RVS (11.9 ± 2.4) was normal. Accordingly, global RV performance quantified by RIMP (0.45 ± 0.11) was also normal. Compared to pre-CABG, TAPSE (14.6 ± 3.7, P<0.001) and RVS (8.5 ± 1.9) deteriorated following CABG. On the other hand, RIMP (0.38 ± 0.08) improved after CABG (Fig. 24). The results of echocardiographic measurements of RV function at rest and peak DSE are shown in Tables 4 and 5.

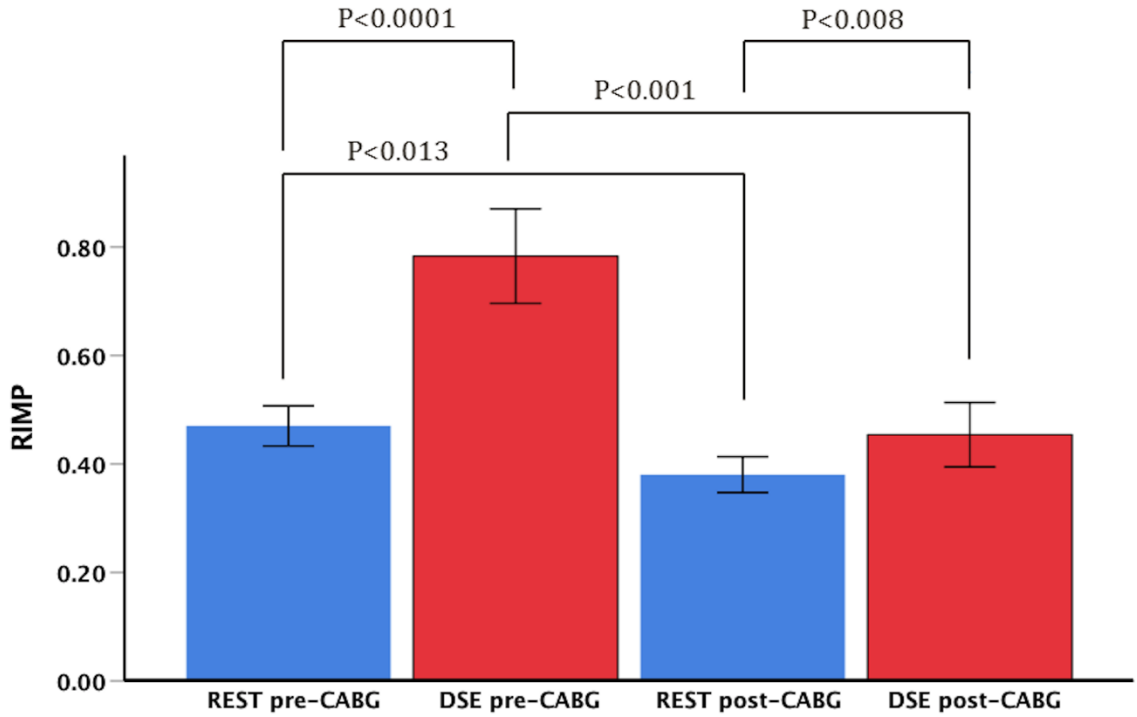

Figure 24. Alterations in RIMP from rest to peak DSE before and after CABG. RIMP: right ventricular index of myocardial performance; CABG: Coronary artery bypass grafting; DSE dobutamine stress echocardiography

Table 4. Echocardiographic assessment of right ventricular size and function at rest before and after CABG (n=42)

Parameter	Rest Pre-CABG	Rest Post-CABG	P-value
RIMP	0.45 ± 0.11	0.38 ± 0.08	0.013
RV systolic function			
TAPSE (mm)	23.9 ± 4.5	14.6 ± 3.6	<0.001
RV peak systolic velocity (S´, cm/s)	11.9 ± 2.4	8.5 ± 1.9	<0.001
RV diastolic function			
Tricuspid peak E-wave velocity (E, m/s)	0.43 ± 0.09	0.46 ± 0.13	0.18
Tricuspid peak A-wave velocity (A, m/s)	0.38 ± 0.07	0.5 ± 0.76	0.33
Tricuspid E/A ratio	1.2 ± 0.33	1.2 ± 0.38	0.69
RV early diastolic velocity (e´, cm/s)	11.4 ± 3.01	8.0 ± 2.80	<0.001
RV late diastolic velocity (a´, cm/s)	13.7 ± 3.50	8.4 ± 2.87	<0.001
RV E/e' ratio	4.1 ± 1.32	6.3 ± 2.69	<0.001
Cardiac time intervals (PW-DTI):			
RV IVCT (ms)	72.1 ± 17.17	63.5 ± 13.52	0.005
RV ET (ms)	307 ± 36.65	306 ± 35.25	0.84
RV IVRT (ms)	67 ± 25.29	57 ± 25.23	0.038
Heart rate (beats/min)	58 ± 9	61±14	<0.05

Data is presented as mean ± SD; CABG: coronary artery bypass grafting; RIMP: right ventricular index of myocardial performance; RV: right ventricle; TAPSE: tricuspid annular plane systolic excursion; S: peak annular longitudinal tissue velocity; E: peak early inflow velocity; A: peak late inflow velocity; E' (early) and A' (late): peak annular longitudinal tissue velocity; IVCT: Isovolumic contraction time; ET: Ejection time; IVRT: Isovolumic relaxation time.

Table 5. Echocardiographic assessment of right ventricular size and function at peak DSE before and after CABG (n=42)

Parameter	Peak DSE Pre-CABG	peak DSE Post-CABG	P-value
RIMP	0.75 ± 0.23	0.49 ± 0.14	<0.001
RV systolic function			
TAPSE (mm)	20.9 ± 4.2	11.9 ± 3.6	<0.001
RV S´(cm/s)	15.6 ± 4.3	10.5 ± 3.2	<0.001
RV diastolic function			
Tricuspid E (m/s)	0.49 ± 0.11	0.67 ± 0.12	<0.001
Tricuspid (A, m/s)	0.59 ± 0.19	0.63 ± 0.22	0.32
Tricuspid E/A ratio	0.88 ± 0.23	1.1 ± 0.29	0.001
RV e´ (cm/s)	13.8 ± 5.10	10.6 ± 4.10	<0.001
RV (a´, cm/s)	19.4 ± 5.05	13.7 ± 3.53	<0.001
RV E/e' ratio	4.2 ± 1.81	7.5 ± 2.81	0.001
Cardiac time intervals (PW-DTI):			
RV IVCT (ms)	62 ± 17.75	47 ± 16.56)	0.020
RV ET (ms)	196 ± 32.12	205 ± 39.05	0.15
RV IVRT (ms)	82 ± 34.01	51 ± 21.49	0.004
Heart rate (beats/min)	126 ± 14	130 ± 18	0.952

Data is presented as mean ± SD; DSE: dobutamin stress echocardiography; CABG: coronary artery bypass grafting; RIMP: right ventricular index of myocardial performance; RV: right ventricle; TAPSE: tricuspid annular plane systolic excursion; S: peak annular longitudinal tissue velocity; E: peak early inflow velocity; A: peak late inflow velocity; E' (early) and A' (late): peak annular longitudinal tissue velocity; IVCT: Isovolumic contraction time; ET: Ejection time; IVRT: Isovolumic relaxation time.

4.3 STUDY III

Forty patients were enrolled in the study. Twenty patients were randomized to MIAVR and 20 patients to AVR. One patient who was randomized to MIAVR, crossed over to AVR due to difficulties in cardioplegia during surgery. Following surgery, 2 (10.5%) patients in the AVR group died. One patient died on day 2, post surgery due to pancreatitis and multi organ dysfunction and one patient died on day 4 due to undiagnosed liver cirrhosis. Finally, 19 patients remained in each group and analyzed. The patients were analyzed as treated. Mean age was marginally but not significantly higher in the AVR as compared to MIAVR (70.8 ± 8.0 vs 67.3 ± 9.0, P = 0.22). At baseline, there were not any significant differences in comorbidities (i.e. Hypertension; Diabetes; Previous stroke; previous coronary artery intervention and renal failure) between the groups (Table 6). Accordingly, baseline medication was similar between the 2 groups both before and after aortic valve replacement surgery. However, the cardiopulmonary bypass time was significantly longer in the MIAVR arm (113.4 ± 36.0 vs 88.7 ± 28.2, P = 0.04), (Table 7).

Table 6. Baseline Clinical Characteristics (n=38)

Patient characteristics	Total (n=38)	AVR (n=19)	MIAVR (n=19)	P-value
Female gender	15 (39.5%)	8 (42.1%)	7 (38.8%)	0.74
Age (years), mean (SD)	70 (9)	70.8 (8)	67.3 (9)	0.22
Body mass index (kg/m^2), mean (SD)	27.9 (5.1)	28.0 (5.9)	27.8 (4.4)	0.55
Systolic blood pressure (mmHg), mean (SD)	133 (16)	132 (13)	134(20)	0.70
Diastolic blood pressure (mmHg), mean (SD)	73 (9)	72 (10)	73 (8)	0.89
Hypertension	25 (65.8%)	13(68.4%)	12 (63.2%)	0.73
Diabetes mellitus	9 (23.7%)	5 (26.3%)	4 (21.1%)	0.70
Insulin-dependent	5 (13.1%)	1 (5.3%)	4 (21.0%)	0.08
Hyperlipideamia	14 (36.8%)	6 (31.6%)	8 (42.1%)	0.50
Chronic pulmonary disease	2 (5.3%)	0	2 (10.5%)	0.08
Previous stroke	2 (5.3%)	2 (10.5%)	0	0.15
Previous PCI	1 (2.6%)	0	1 (5.3%)	0.31
Renal failure	2 (5.3%)	0	2 (10.5%)	0.15
ECG				
LBBB/RBBB	4 (10.5%)	3 (15.8%)	1 (5.3%)	0.15

Values are presented as n (%) unless otherwise noted. PCI: percutaneous coronary intervention. LBBB: left bundle branch block; RBBB: right bundle branch block.

Table 7: Perioperative data (n=38)

Parameter	AVR (n=19)	MIAVR (n=19)	P-value	Total (n=38)
Cardio pulmonary bypass time (min)	88.7 ± 28.2	113.4 ± 36	0.040	102 ± 35
Aorta cross clamp time (min)	70.7 ± 22	82.9 ± 26.9	0.72	77 ± 25
Valve type				
Biological prosthesis	14 (73.7%)	14 (73.7%)	0.72	29 (72%)
Mechanical prosthesis	5 (26.3%)	5 (26.3.6%)	0.72	10 (25%)
Sutureless	0	7 (36.8%)	0.003	7 (18.4%)
valve size (mm)	23 ± 1.3	23 ± 1.7	0.070	23 ± 1.6
De novo pacemaker	1 (5.3%)	0	0.40	1 (2.6%)
PEX day 1	7 (36.8%)	10 (52.6%)	0.48	17 (44.7%)
PEX day 4	15 (78.9%)	16 (84.2%)	0.72	31 (81.6%)
Tamponade	1 (5.2%)	2 (10.5%)	0.62	3 (7.9%)
30 days Mortality	2 (10%)	0	0.22	2 (5.2%)

Data is expressed as mean ± SD or number (%). AVR: aortic valve replacement; MIAVR: minimally invasive aortic valve replacement; PEX: pericardial exudate.

4.3.1 Impact of AVR and MIAVR on right heart size and function

The RV 2D size remained unchanged following both AVR and MIAVR. On the other hand compared to pre-surgery values, RV systolic function was deteriorated following both AVR and MIAVR. Compared to pre-surgery, TAPSE decreased following AVR (26.1 ± 4.6 vs 15.6 ± 3.3; P<0.0001) as well as following MIAVR (24.8 ± 3.7 vs 19.2 ± 3.8; P = 0.001). Although, the magnitude of post-surgical reduction in TAPSE was significantly higher post-AVR (39.9%) as compared to post-MIAVR (21.6%, P = 0.007 (Fig. 25). Accordingly, RVS declined following surgery as compared to pre-surgery both following AVR (9.3 ± 2.1 vs 5.9 ± 1.5; P<0.01) and following MIAVR (10.1 ± 2.9 vs 8.2 ± 1.4, P<0.01). Similarly the magnitude of post-surgical reduction in RVS was significantly higher post-AVR (36.6%) as compared to MIAVR (18.8%; P<0.001).

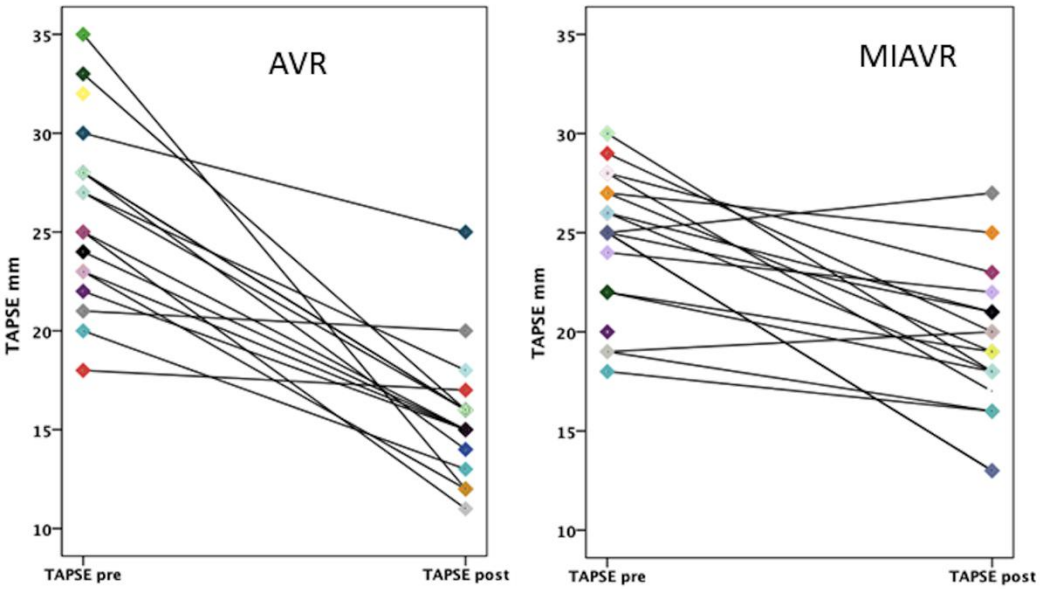

Figure 25. Changes in TAPSE following aortic valve replacement surgery. TAPSE: tricuspid annular systolic excursion, AVR: aortic valve replacement surgery; MIAVR: minimal invasive aortic valve replacement surgery.

Prior to surgery, RVFAC was normal in the AVR-group (54.3 ± 7.7%) as well as in the MIAVR-group (55.5 ± 6.4%). Following surgery, a significant reduction in RVFAC was observed in both AVR (47.7 ± 11.2%; P<0.01) and MIAVR (51 ± 8.5%; P<0.05). However, in both groups RV FAC still remained within the normal range following surgery. Prior to surgery, no significant difference in RV performance as quantified by RIMP was observed. After surgery, RIMP was equally deteriorated (prolonged) in both groups (AVR (33.3%) vs MIAVR (30.8%); P = 0.25). Before surgery, RV-LS and RV-LSR were within normal range and without any significant differences between the groups. After surgery, RV-LS was equally deteriorated in both groups. On comparing pre- to post surgery values, RV-LSR was deteriorated following AVR (-1.7 ± 0.3 1/s vs -1.4 ± 0.3; P<0.01), while it was preserved following MIAVR (-1.5 ± 0.5 vs -1.5 ± 0.4 1/s; P = 0.84), (Table 8). Echocardiographic characteristics of LV size and function before and after aortic valve replacement surgery in the two surgical groups is displayed in Table 9.

Table 8. Pre- and postoperative echocardiographic assessment of right heart size and function in the two surgical groups

	Before aortic valve surgery		**After aortic valve surgery**		**P-value**	
Echocardiographic Parameter	AVR	MIAVR	AVR	MIAVR	Between the groups pre†	Between the groups post†
TAPSE (mm)	26.26 ± 4.5	24.5 ± 3.6	15.8 ± 3.2***	19.2 ± 3.8***	0.20	**0.005**
RVS (cm/s)	9.3 ± 2.1	10.1 ± 2.9	5.9 ± 1.5**	8.2 ± 1.4**	0.39	**< 0.001**
RVE´ (cm/s)	8.4 ± 2.9	7.1 ± 2.1	4.7 ± 2.9**	4.7 ± 2***	0.14	0.99
RVA´ (cm/s)	12.2 ± 3.5	12.2 ± 2.9	4.9 ± 1.9**	9 ± 3.2***	0.97	**< 0.01**
RV E´/A´	0.84 ± 0.61	0.6 ± 0.21	1.1 ± 0.9	0.55 ± 0.3	0.17	**0.04**
FAC (%)	54.3 ± 7.7	55.5 ± 6.4	**47.7 ± 11.2****	**51 ± 8.5***	0.70	0.56
RV longitudinal strain (%)	-27.4 ± 3	-26.5 ± 5.3	**-18.8 ± 4.7*****	**-20.7 ± 4.5****	0.56	0.25
RV strain rate (1/s)	-1.7 ± 0.3	-1.6 ± 0.3	**-1.4 ± 0.3****	-1.5 ± 0.4	0.65	0.53
RIMP	0.75 ± 0.2	0.68 ± 0.16	1 ± 0.4**	**0.89 ± 0.2****	0.26	0.25
PEP (ms)	123.1 ± 62	104 ± 29	136 ± 29	129 ± 41*	0.25	0.69
ET (ms)	300.5 ± 40	308.7 ± 37	256.2 ± 49*	267.4 ± 54*	0.54	0.56
POP (ms)	100 ± 27	103.7 ± 25	116 ± 30	100 ± 35	0.74	0.19
RVOT prox (mm)	30.06 ± 3.2	30.2 ± 3.9	29.2 ± 3.9	29.2 ± 4.2	0.84	0.79
RVD1 (mm)	31.05± 4	32.1± 4.4	32.3 ± 4.7*	33.5 ± 3.4*	0.75	0.39
RA volume (ml)	40.3 ± 16.7	42.6 ± 16.1	45.3± 20.8*	45.1 ± 14.7*	0.16	0.40
TR Vmax (m/s)	2.7 ± 0.4	2.5 ± 0.87	1.9 ± 1.1*	1.7 ± 1.1	0.54	0.67
SPAP (mmHg)	37.5 ± 9.1	31.7 ± 13.7	27.9 ± 6.7*	22.8 ± 13.6	0.76	0.62
HR (min^{-1})	69.6 ± 12	63.4 ± 9.1	72.5 ± 13.7*	71.2 ± 13*	0.22	0.75

RV: right ventricle; AVR: aortic valve replacement; MIAVR: minimally invasive aortic valve replacement; TAPSE: tricuspid annulus systolic excursion; S: peak systolic myocardial velocity; E´: early diastolic myocardial velocity; A´: late diastolic myocardial velocity; FAC: fractional area change; RIMP: right ventricular index of myocardial performance; PEP: pre ejection period; ET: ejection time; POP: post ejection time; RVOT prox: proximal RV outflow diameter; RVD1: RV basal linear dimension; RA: right atrial; TR: tricuspid regurgitation; SPAP: systolic pulmonary artery pressure; HR: heart rate.

Paired t test vs baseline:

* $p < 0.05$.

** $p < 0.01$.

*** $p < 0.001$.

† Independent samples t-test to compare degree of changes between AVR and following MIAVR.

Table 9. Pre- and postoperative echocardiographic assessment of left heart size and function in the two surgical groups.

	Before aortic valve surgery		Post aortic valve surgery		P-value	
Parameter	AVR	MIAVR	AVR	MIAVR	Between the groups pre†	Between the groups post†
LVEDD (mm)	44.8 ± 5.1	46.3 ± 5.3	43.65 ± 4.9*	47.1 ± 5.6	0.67	0.03
LVESD (mm)	26.9 ± 6.2	28.7 ± 6.9	26.7 ± 5.1	30.6 ± 6.9	0.40	0.03
LVEDV (ml)	85.6 ± 19.9	102 ± 30	82 ± 17.2	100.5 ± 29.7	0.14	0.03
LVESV (ml)	34.9 ± 10.4	42.3 ± 13.3	36.1 ± 10.4	45.5 ± 14.9	0.11	0.04
LVEF (%)	60.2 ± 5.7	57.8 ± 6.3	56.5 ± 5.4**	54.6 ± 6.5	0.33	0.37
LVGLS (%)	-16.5 ± 8.1	-17.4 ± 2.1	-15.7 ± 2.7	-16.9 ± 2.1	0.64	0.21
LVMPI	0.81 ± 0.26	0.75 ± 0.16	0.91 ± 0.18	0.89 ± 0.15**	0.37	0.63
Mitral E (m/s)	0.81 ± 0.31	0.8 ± 0.27	0.84 ± 0.23	0.89 ± 0.29	0.72	0.71
Mitral A (m/s)	0.98 ± 0.37	0.81 ± 0.36	0.89 ± 0.28*	0.79 ± 0.26	0.14	0.61
Mitral E/A	0.84 ± 0.22	1.2 ± 0.86	0.98 ± 0.27	1.2 ± 0.43	0.14	0.46
Dec T (ms)	228.8 ± 61	201.1 ± 58.4	200 ± 50	203.7 ± 49.7	0.30	0.59
LA volume (ml)	83.2 ± 23.3	79.6 ± 20.5	75.2 ± 22.1	79.8 ± 23.7	0.53	0.58
HR (min^{-1})	69.6 ± 12	63.4 ± 9.1	72.5 ± 13.7*	71.2 ± 13*	0.22	0.75

LV: left ventricle; EDD: end diastolic diameter, ESD: end systolic diameter; EDV: end diastolic volume; ESV: end systolic volume; EF: ejection fraction; GLS: global longitudinal strain; MPI: myocardial performance index; E: early diastolic flow velocity; A: late diastolic flow velocity; Dec T: deceleration time; LA: left atrium; HR: heart rate.

Paired t test vs baseline:

* $p < 0.05$.

** $p < 0.01$.

*** $p < 0.001$.

† Independent samples t-test to compare degree of changes between AVR and MIAVR.

4.4 STUDY IV

4.4.1 TOTAL COHORT

Eighty-eight patients were included in the study of which, 13 (14.8%) were females. Mean age was (63.8 ± 9.0). The number of patients with diabetes was 21 (23.9%); hypertension 36 (40.9%); hyperlipidemia 80 (90.9%), previous MI 48 (54.5%). Eighteen (20.5%) patients were smokers (Table 10).

During the follow up period of 5 years after CABG, major adverse cardiovascular events (MACE) was observed in 17 (19.3%) patients: 6 (6.8%) patients died; 8 (9.1%) patients were treated with PCI of which 5 patients suffered from MI; and 3 patients were treated for congestive heart failure (CHF).

On comparing to patients without MACEs, patients experiencing MACEs were significantly older (62.7 ± 8.7 vs 67.3 ± 9.2; P = 0.028) and had moderately impaired renal function (creatinine clearance: 68.2 ± 17.6 vs 84.0 ± 12.0 ml/min; P = 0.006). In addition, larger proportion of patients experiencing MACEs had hypertension as compared to those without MACEs (36 (40.9%) vs 23 (34.3%); P = 0.025).

On comparing medication between the 2 groups, before CABG a higher proportion of patients who did not experience MACEs were treated with Beta-blockers (70.6% vs 91.0 %; P = 0.009). However, after CABG there was no significant difference between the 2 groups' beta blocker treatment. On the other hand, lower proportion of patients experiencing MACEs were treated with statins as compared to those without any events (76.5% vs 95.8%; P = 0.008).

Seventy four (84.1%) patients underwent follow-up angiography 3 months after CABG . Twenty-two (29.7%) patients had one or more occluded grafts. There was no significant difference in BNP values comparing patients with- or without graft-occlusion (524 [quartile 1: 208, quartile 3: 1099].vs 272 [1:160, 556]; P=0.267).

4.4.2 Subpopulation of patients with DTI

Forty patients were analyzed in the subpopulation. A total of 10 (25%) patients experienced MACEs during the 5 years of follow-up: 4 (10.0%) patients died, 3 (7.5%) patients were treated for AMI, 1 (2.5%) patient was treated for heart failure and 5 (12.5%) patients underwent PCI. There was no

significant difference in co-morbidities or medications between those who experienced MACEs and those who did not (Table 2).

Table 10. Baseline clinical characteristics in total cohort (n=88)

Patient characteristics	Patients without MACEs (n=71)	Patients with MACEs (n=17)	P Value
Male/Female, n(%)	57 (80.28)/10 (14.08)	18 (85.71%)/3 (14.29%)	0.9
Age (years), (SD)	62.75 (8.67)	67.33 (9.24)	**0.0**
Body mass Index (kg/m2)	35.29 (2.94)	32.99 (2.89)	0.7
Diabetes, n(%)	18 (26.86%)	3 (14.29%)	0.2
Hypertension, n(%)	23 (34.32%)	13 (61.90%)	**0.0**
Hyperlipidemia, n(%)	62 (92.54%)	18 (85.71%)	0.3
Creatinine Clearance (ml/min), (SD)	84.02 (21.01)	68.17 (17.58)	**0.0**
Previous myocardial infarction, n(%)	34 (57.75)	14 (66.67%)	0.2
Smoker, n(%)	15 (22.39%)	3 (14.29%)	0.4
Ex-smoker (> 3 months), n(%)	24 (35.82%)	9 (42.86%)	0.6
Systolic Blood pressure (mmHg), (SD)	142.05 (18.75)	149.05 (15.86)	0.1
Diastolic Blood Pressure (mmHg), (SD)	81.44 (10.59)	83.33 (8.71)	0.5

Data is presented as n (%): number of patients with percentages in parentheses or mean (SD); SD: Standard deviation.

4.4.3 BNP and echocardiographic measurements in overall population

Generally compared with baseline, plasma BNP concentration (median: 311 [quartile 1: 147, quartile 3: 571] pg/ml), increased significantly after CABG (387 [182.8, 779] pg/ml; P = 0.038) and a significant correlation between pre- and post-CABG BNP concentrations was observed (r = 0.57: P<0.0001). On comparing patients with- and without MACEs, BNP levels were significantly higher in patients with MACEs, both prior to CABG (464 [289.5, 632.5] pg/ml vs. 268 [143, 555] pg/ml: P = 0.027) and post-CABG (1096 [754, 1684.5] vs. 299 [170, 558] pg/ml; P<0.0001), (Fig. 26). Accordingly, among the patients experiencing MACEs, BNP levels increased significantly post-CABG as compared to baseline (464 [289.5, 632.5] pg/ml vs. 1096 [754 vs. 1684.5] pg/ml; P = 0.015), (Table 11).

Table 11. BNP and echocardiographic measurements in patients with and without events in total cohort, before and after CABG

Parameter	No Event pre (n=71)	Event pre (n=17)	P Value	No Event post (n=71)	Event post (n=17)	P Value
BNP (ng/L)	477.14 ± 601.26 268(143, 555)	702.82 ± 879.83 464 (289.5, 632.5)	**0.027**	442.04 ± 459.91 299 (170, 558)	1253.41 ± 1080.77 1096 (754, 1684.5)	**<0.0001**
EF (%)	43.01 ± 8.1 43 (37, 48.25)	41.93 ± 7.48 40 (38, 48)	0.433	43.88 ± 7.92 43 (40, 49)	42.25 ± 8.83 43 (36.75, 46.5)	0.44
Mitral E/A	1.04 ± 0.47 0.89 (0.8, 1.2)	0.89 ± 0.29 0.75 (0.71, 1.17)	0.124	1.20 ± 0.56 1.0 (0.83, 1.5)	1.3 ± 0.77 0.94 (0.79, 2.05)	0.942
Mitral E/E'	9.61 ± 6.59 8.01 (6.77, 10.5)	9.92 ± 3.89 8.3 (6.67, 14.29)	0.561	8.04 ± 2.45 7.91 (6.25, 9.75)	9.74 ± 3.88 9.41 (6.75, 11.99)	0.067
Tri. E/A	1.19 ± 0.31 1.15 (1, 1.33)	1.15 ± 0.26 1.20 (1, 1.29)	0.655	1.27 ± 0.40 1.25 (1.0, 1.40)	1.35 ± 0.34 1.33 (1.25, 1.43)	0.870
Tri. E/E'	4.15 ± 1.35 3.75 (3.08, 5.)	3.68 ± 1.13 3.57 (2.85, 4.)	0.367	6.32 ± 2.69 6.30 (4.35, 7.32)	5.65 ± 1.45 5.71 (4.55, 6.46)	0.401
HR (beat/min)	61.86 ± 12.94 59 (51, 63)	63.31 ± 12.34 62 (52, 80)	0.619	67.30 ± 15.03 64 (58.5, 72)	65.73 ± 12.29 63 (56, 76)	0.447

Data is presented as mean ± SD and median (quartile 1, quartile 3).
BNP: B-type natriuretic peptide; EF: Ejection fraction; E: early diastolic flow velocity; E`: early diastolic tissue velocity, Tri: Tricuspid; HR: Heart rate; CABG: coronary, artery bypass grafting.
Pre: before CABG; post: after CABG.

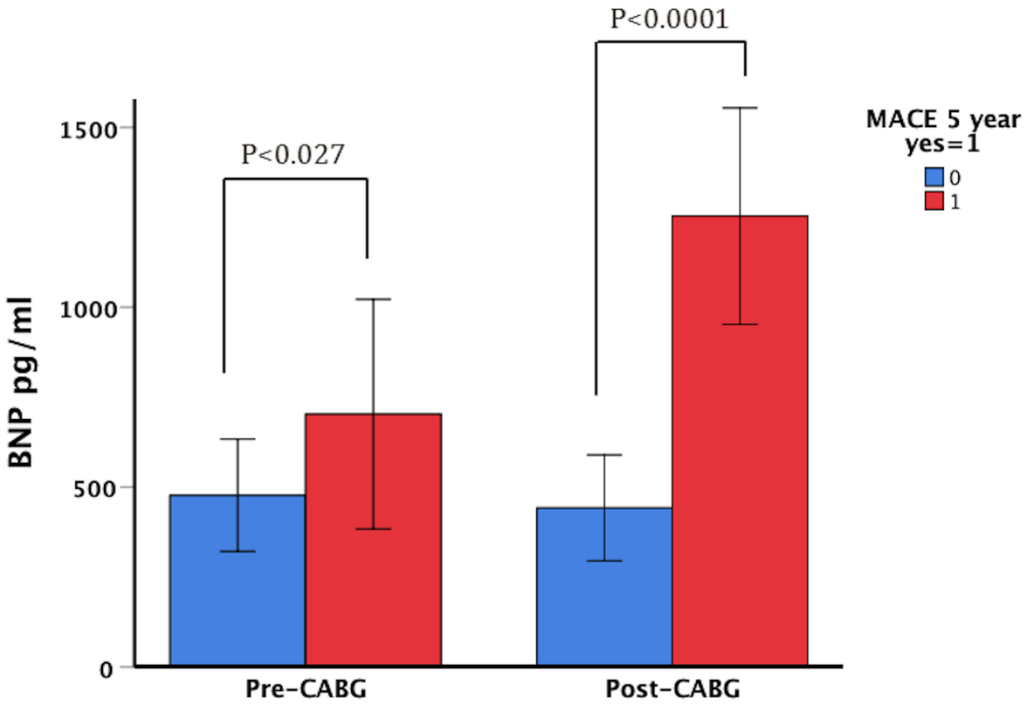

Figure 26. BNP levels in patients with and without MACEs in total cohort, assessed before and after CABG. BNP: Brain natriuretic peptide, CABG: Coronary artery bypass grafting.

4.4.4 BNP and echocardiographic measurements in subpopulation

In the subpopulation, a total of 40 patients were analyzed. The alteration in BNP level in the subpopulation after CABG was similar to the total population. Compared with baseline values plasma BNP concentration (median: 272 [quartile 1: 109.5, quartile 3: 476.8] pg/ml), increased significantly after CABG (386.5 [173, 1091] pg/ml; P = 0.002). Analyzing the BNP levels among the patients in the subpopulation with MACEs compared to those without, a significantly higher level of BNP was measured pre-CABG (472 [300.8, 604.8] pg/ml vs. 219.5 [98.0, 380.3] pg/ml: P = 0.024). Accordingly, patients with MACEs had significantly higher levels of BNP post-CABG as compared to baseline (1160 [1009.8, 1637.8] pg/ml vs. 246 [155.8 vs. 460.8] pg/ml; P = 0.001), (Table 12).

Table 12. Comparison of BNP and echocardiographic measurements in patients with and without events in the subpopulation of patients with DTI-measurements , before and after CABG

Parameter	No Event pre (n=30)	Event pre (n=10)	P Value	No Event post (n=30)	Event post (n=10)	P Value
BNP (pg/ml)	356.2 ± 480.8 219.5 (98, 380.25)	510.9 ± 332.5 472(300.8, 604.8)	**0.024**	435.5 ± 565.4 246 (155.8, 460.8)	1180.3 ± 506.5 1160 (1009.8, 1637.8)	**0.001**
LVMPI	0.60 ± 0.11 0.59 (0.53, 0.68)	0.61 ± 0.14 0.6 (0.54, 0.65)	0.890	0.43 ± 0.08 0.44 (0.38, 0.48)	0.49 ± 0.07 0.49 (0.40, 0.54)	0.891
RIMP	0.44 ± 0.11 0.44 (0.38, 0.53)	0.44 ± 0.12 0.49 (0.37, 0.51)	0.883	0.39 ± 0.11 0.38 (0.30, 0.45)	0.41 ± 0.08 0.39 (0.37, 0.43)	0.649
EF (%)	42.51 ± 7.66 42 (38, 47)	44.06 ± 9.2 44 (35.5, 50.5)	0.632	43.90 ± 8.29 43 (39.25, 49)	42.29 ± 7.14 43 (40.5, 44.5)	0.590
Mitral E/A	1.05 ± 0.54 0.88 (0.79, 1.22)	1 ± 0.33 1 (0.69, 1.33)	0.973	1.30 ± 0.71 1.18 (0.79, 1.61)	1.46 ± 0.78 1.16 (0.86, 2.41)	0.660
Mitral E/E'	9 ± 2.79 9.33 (6.76, 10.89)	10.29 ± 4.25 9.04 (6.1714.51)	0.566	8.57 ± 2.59 8.42 (6.4, 10.39)	9.42 ± 2.72 9.64 (6.59, 11.34)	0.334
Tri. E/A	1.24 ± 0.33 1.25 (1, 1.33)	1.11 ± 0.28 1.13 (0.90, 1.24)	0.240	1.22 ± 0.39 1.25 (1, 1.33)	1.2 ± 0.22 1.25 (1, 1.33)	0.775
Tri. E/E'	4.22 ± 1.31 4 (3.12, 5.45)	3.33 ± 0.63 3.57 (2.85, 3.70)	0.136	6.45 ± 3 6.51 (4.29, 7.89)	5.74 ± 1.56 5.83 (4.55, 6.69)	0.639
HR (beat/min)	58.64 ± 8.16 58.5 (51.25, 66)	61.56 ± 10.96 60 (52.5, 70)	0.946	64.92 ± 12.29 65 (60, 69)	59.56 ± 8.53 66 (53.75, 75.25)	0.305

Data is presented as mean ± SD and median (quartile 1, quartile 3).
BNP: B-type natriuretic peptide; EF: Ejection fraction; E: early diastolic flow velocity; E`: early diastolic tissue velocity; Tri: Tricuspid; HR: Heart rate; CABG: coronary, artery bypass grafting.
Pre: before CABG; post: after CABG.

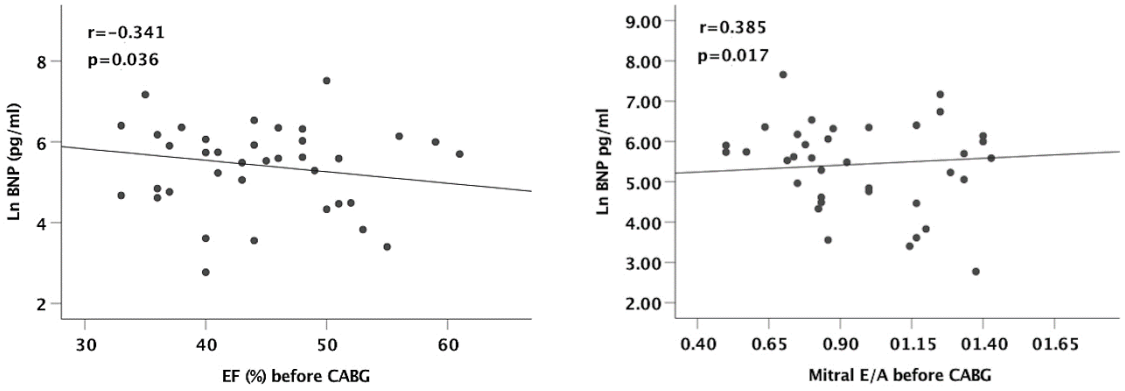

Figure 27. Correlation between Ln BNP –LVEF and Ln BNP-Mitral E/A, before CABG: BNP: brain natriuretic peptide, EF: Ejection fraction; E: Early diastolic flow velocity; A: Late diastolic flow velocity; CABG: Coronary artery bypass grafting.

A significant, negative correlation between preoperative BNP and preoperative EF was revealed (r = -0.34; P = 0.036), (Fig. 27). A significant, positive correlation between preoperative BNP and preoperative LV-MPI (r = 0.531; P<0.001); and preoperative BNP and preoperative RIMP (r = 0.335; P = 0.032) was observed (Fig.28). However, no significant correlation between postoperative BNP and postoperative LVMPI, postoperative RIMP and postoperative EF respectively could be revealed.

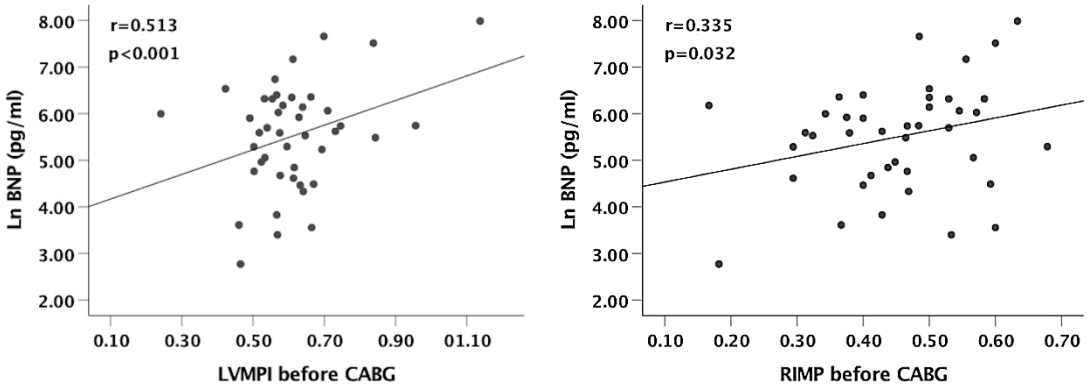

Figure 28. Correlation between Ln BNP –LVMPI and Ln BNP-RIMP, before CABG: BNP: brain natriuretic peptide, LVMPI: left ventricular myocardial performance index; RIMP: Right ventricular index of myocardial performance; CABG: Coronary artery bypass grafting

4.4.5 Cut-off values of postoperative BNP for detection of events

Using ROC-curve cut-off level for postoperative BNP was assessed (Fig 29). A cut-off level of 602-761 pg/ml was considered optimal based on a sensitivity of 80.3%-76.5% and a specificity of 80.3%-87.3% for predicting MACEs 5 year after CABG. The accuracy of postoperative BNP in predicting MACEs was 84.1%.

Among clinical and echocardiographic variables that were analyzed in a univariate regression model postoperative BNP (P = 0.001), preoperative BMI (P = 0.01), pre- and postoperative creatinine clearance (P = 0.01 and P = 0.01), postoperative statins (P = 0.02) and preoperative beta-blockers (P = 0.02) were all significantly associated with the incident of MACEs at follow-up. Further analysis of the above variables in a multivariate logistic regression model revealed that postoperative BNP (P = 0.003) and preoperative BMI (P = 0.025) were independent predictors of MACEs.

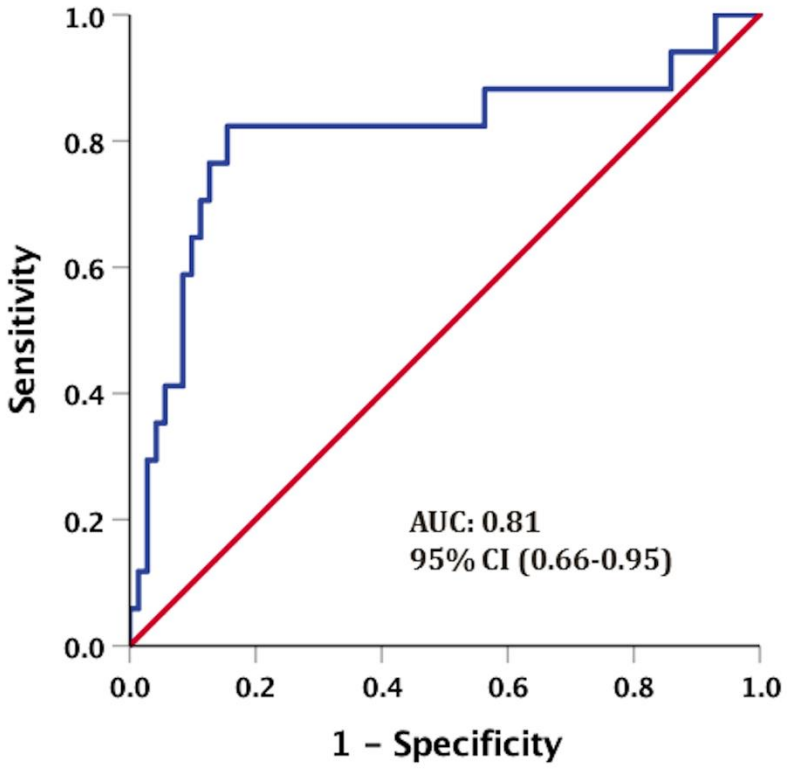

Figure 29. ROC-curve displaying sensitivity and specificity of postoperative BNP in detection of MACES. AUC: Area under the curve; CI: Confidence interval; BNP: Brain natriuretic peptide; MACES: Major adverse cardiovascular events.

5 GENERAL DISCUSSION

Our studies reveal that despite advances in echocardiographic technology, controversies still remain in echocardiographic evaluation of cardiac function following open heart surgery. The reason is complex and multifactorial. However, one of the main reasons may be altered cardiac motion due to altered geometry and loss of pericardial constraint following opening of the pericardium in open heart surgery (79, 80). A number of surrogate parameters of RV function are one-dimensional measurements and influenced by cardiac translational motion resulting in an underestimation of RV function following heart surgery (81). Further, several echocardiographic modalities are angel-dependent, thus changes in cardiac geometric location in the chest may influence their results. The key to overcoming these shortcomings is to include several modalities for assessment of cardiac function and not rely on a sole metric. This is especially important in determining RV function following open heart surgery. It is recognized that RV movement along its longitudinal axis as assessed by RVS and TAPSE declines after open heart surgery (79, 82). However, the interpretation of these findings has been extremely divergent. While some studies have reported deterioration in global RV function amid reduced longitudinal RV movement (83), other studies using other modalities for assessment of RV function have reported preserved global RV function despite a post-surgical reduction in RV longitudinal function (84). In study II, our results confirm previous findings of reduction in RV longitudinal function following CABG (83), (85). However, we observed an improvement in global RV performance as assessed by RIMP both at rest and during DSE. Concomitantly, we observed improvements in patients' clinical parameters following CABG. Consistent with previous studies (86), in our study the prevalence of angina dropped dramatically and the use of anti-angina medication reduced significantly (87). Accordingly, follow-up angiography demonstrated patent grafts to RCA, CX and other coronary arteries in the majority of patients. In addition, following CABG, exercise capacity improved significantly in the majority of the patients and the reason for ending the bicycle exercise test was fatigue, not angina. In conclusion, the cohorts' clinical parameters improved significantly following CABG, while concurrently the RV longitudinal function diminished. Previously, it has been demonstrated that RV function is one of the major determinants of exercise capacity (88). The paradox of improved exercise capacity and reduced global RV performance doesn't fit together. Rather, in this clinical setting, the improvement in global RV performance sounds more reasonable.

Accordingly, in study III, a reduction in longitudinal RV function following both AVR and MIAVR was observed. However, the magnitude of the reduction in longitudinal RV function was significantly higher following full sternotomy AVR. The results suggest that the accurate assessment of RV longitudinal motion using conventional TAPSE and RVS is dependent upon the intact myocardium (80). Even smaller openings of the myocardium may result in geometrical alterations and subsequently the alterations in RV longitudinal motion. However, according to previous studies the location of the pericardial opening is also crucial in whether it results in reduction of longitudinal RV function or not (89). In study III, global RV performance assessed by RIMP (prolonged), RVFAC, and RV-LS, were equally impaired following both AVR and MIAVR. The only RV echocardiographic parameter that diverged between AVR and MIAVR was RV-LSR. LSR has shown to be the best measure of intrinsic myocardial contractility (90, 91). Our findings demonstrate that myocardial contractility was preserved following MIAVR but not following AVR, despite longer cardiopulmonary bypass time in the MIAVR arm. In addition, the stroke volume was preserved following MIAVR but decreased following AVR, further strengthening our findings.

In contrast to study II, RIMP was deteriorated (prolonged) in study III. The difference in the state of myocardial ischemia between these two studies might provide an explanation for the diversion in RIMP alterations. In study II, the majority of patients had 3-vessel disease and significant ischemia was revealed on DSE, while in study III patients with significant ischemia and requiring CABG were excluded from the study. Thus, RIMP might rather measure the burden of ischemia on myocardial function.

In study I, using MPI assessed by PW-DTI of four different sites around the basal portion of the LV, an improvement in global LV performance was observed post-CABG at both rest and peak DSE. In contrast to MPI, traditional measures of LV function such as WMSI and LVEF did not improve at rest following CABG as compared to baseline. Consistent with previous studies, LVEF did not improve at rest following CABG as compared to pre-CABG (92-94). The effect of CABG on LVEF has been divergent in previous studies. While some studies have reported an improvement in resting LVEF following CABG, others have reported no improvement in resting LVEF, but improvement in LVEF only during stress (93, 94). Several factors have been recognized as important determinants of improvement in LVEF after CABG. Substantial myocardial viability has been regarded as a crucial factor to obtaining functional improvement after CABG. However, in some studies that only included patients with substantial amount of viable myocardium, resting LVEF did not improve in 48% of the cohort following CABG. On the

other hand, in these patients peak stress LVEF improved following CABG (92). Additional factors influencing recovery in LVEF include: i) presence of extensive scar tissue which might prevent an increase in LVEF despite viable myocardium(95); and ii) graft occlusion after CABG which may hamper cardiac functional recovery of viable myocardium following CABG (96). Improvement in LV function at rest has previously been considered an indicator for the success of CABG in patients with advanced CAD (94). Considering the above mentioned limitations of LVEF to quantify improvement in LV functional recovery following CABG, MPI may have an incremental value in the assessment of LV function after CABG.

In study IV, we demonstrate that postoperative BNP with a cut-off value of 602-761 pg/ml, at 3-months after CABG and in a stable clinical setting, is a strong predictor of MACEs 5 years after CABG. Patients who had MACEs at 5-years follow-up had significantly higher levels of BNP compared to patients without events. These results indicate that BNP is a powerful prognostic marker of long-term events following CABG. Our results are partly in accord with the results of previous studies evaluating the role of BNP as a prognostic marker for cardiovascular events in patients after cardiac surgery. Nozohoor et al (97) showed that BNP obtained the first day after CABG predicts one-year mortality. However, in a study by Fellahi et al (98), BNP was analyzed only days after cardiac surgery in a mixed cohort of patients undergoing CABG and aortic valve replacement surgery while patients were still staying in the ICU. The results of this study revealed that early post-surgery BNP is only predictive of events in patients with aortic valve replacement and not in patients with CABG. In another study by Fox et al (99), only pre-operative BNP was an independent predictor of heart failure hospitalization after CABG, while peak early post-operative BNP was not. To our knowledge, the present study is the first one to evaluate the prognostic significance of BNP obtained a few months after CABG and in patients with clinically stable conditions.

In the subpopulation of patients with DTI, a strong correlation between BNP, LVMPI, RIMP and LVEF, respectively, was observed. However, no significant correlation was observed following CABG. We speculate that the state of ischemia prior to CABG might influence RIMP, LVMPI, BNP, and LVEF in the same direction. However, these markers react differently to the relief from the burden of ischemia following revascularization surgery. Cardiac time intervals are sensitive markers of ischemia, while BNP reflects the state of mechanical adaption of the heart. Previous studies show that echocardiographic recovery of cardiac function may take up to one year (100). In study I, no improvement was observed in resting LVEF, while a significant

improvement in LVEF at peak stress was observed. In our study, BNP was analyzed 3 months after CABG, which may be too short for reflecting the adaptive mechanical changes following CABG.

As our knowledge is growing and novel echocardiographic modalities are emerging, our understanding of myocardial function and its physiological response/adaptation to pericardial opening and its functional recovery from burden of ischemia and valvular heart disease is improving.

5.1 LIMITATIONS

The main limitation of study I, and II was lack of a gold standard method reference method for assessment of LV- and RV function such as EF by cardiac magnetic resonance, or EF by 3D echocardiography. We lack a healthy control group to characterize the alterations in RIMP and LV MPI at rest and peak DSE in this group compared to the patients with CAD. However, as patients were examined four times during the course of study, they serve as their own controls. The study cohort was small. However, power calculations had revealed that the size of the cohort would be enough to detect the changes in the examined parameters. Similarly, one of limitations of study III was small sample size. And another was using different cardioplegia strategies between the AVR- and MIAVR group. The pericardium was closed following MIAVR but not following AVR could be mentioned as another limitation since it may influence the result of metrics assessing longitudinal RV function and the follow-up was too short. In study IV, BNP was assessed prior to CABG and at 3 months follow-up. It would have been interesting to assess BNP, also long time after CABG in order follow changes in BNP value over time. Echocardiographic measurements were also assessed 3 months after CABG which may be too short for some parameters to detect changes at rest.

6 CONCLUSIONS

Echocardiographic assessment of cardiac function can in some scenarios be challenging despite advances in the current techniques of echocardiography imaging. While some modalities are perfectly suitable in certain clinical scenarios, they may not be suitable in other situations, due to certain limitations in each modality. Thus, it is important to employ several modalities for assessment of cardiac function. Our studies provide insights into assessment of cardiac function following CABG and surgical aortic valve replacement. While EF is widely used, it has important limitations with moderate accuracy. Further, improvement in LV function following CABG has been used as an echocardiographic marker of successful CABG. Although in study I, as in conjunction with previous studies, EF did not improve despite an improvement in clinical parameters. On the other hand, an improvement in LVMPI was observed. Thus, LVMPI, an expression of different cardiac time intervals may have incremental value in the assessment of cardiac function following CABG.

In Study II; TAPSE and RVS declined following CABG. On the contrary, and consistent with clinical parameters RIMP improved both at rest and at peak DSE following CABG. While TAPSE and RVS represent global RV function under normal conditions, they may not represent global RV function following CABG due to altered cardiac geometry and cardiac motion. Our findings suggest that, RIMP might constitute additional information in the evaluation of RV function following CABG.

In Study III, RV function is a reflection of preload, afterload and contractility. While contractility is the intrinsic myocardial property, preload and afterload are determined by a variety of hemodynamic factors. RV function is sensitive to changes in loading conditions. Further, many of metrics in assessment of RV function are load dependent. In our study, TAPSE and RVS, in conjunction with other load dependent measures of RV function, deteriorated following both AVR and MIAVR. While, less load dependent LSR representing myocardial contractility, remained unchanged following MIAVR but deteriorated following AVR. Our results suggest that an accurate assessment of RV function should both load dependent and load independent metrics.

In study IV, postoperative BNP assessed in a stable clinical setting following CABG, provided a good marker for future MACEs, 5 years after CABG. BNP might provide valuable prognostic information in patients undergoing cardiac surgery and can potentially be incorporated as a diagnostic marker at the regular clinical follow-up of the patients following CABG.

7 FUTURE PERSPECTIVE

Introducing Two-dimensional echocardiography allowed visualization of cardiac structure and function in real time, opened new possibilities in physical examination and revolutionized the patient management. The potential and utility of ultrasound is unlimited and the development has been rapid and multi directional. While the image quality has consistently improved and new modalities are emerging, smaller and smaller ultrasound devices are designed. Currently, ultrasound devices are small enough to fit in the pocket and known as “pocket ultrasounds”, are commercially available. Pocket ultrasounds are gaining popularity among cardiologists. Will future cardiologists carry a stethoscope in one pocket and a “pocket ultrasound” in the other one? Or the development will go so far that the future cardiologist will carry a “pocket ultrasound” along with the stethoscope? More than 200 years ago, the stethoscope, a tube filled with air, which enables conducting sound, replaced direct placement of the ear on the chest. Certainly, the stethoscope revolutionized the diagnostic of cardiac disease at that time. However, in the era of digitalization and an urge for diagnostic accuracy, maybe the role of the stethoscope is going to become limited and the ultrasound will gain new grounds. Furthermore, the future development and implementation of novel pocket Doppler echocardiographic modalities and indexes such as strain, harmonic power, perfusion echocardiography and others, will have a great impact, permitting the rapid advanced assessment and management of patients with cardiovascular diseases

8 ACKNOWLEDGEMENTS

The road toward a doctoral degree is an inspiring and at times tortuous journey for the intellectually curious mind. Through passion, dedication and perseverance the budding investigator acquires an analytic mindset, that is of key importance not only for new discoveries but also to further advancing our evidence based knowledge within clinical medicine.

Just like so many other aspect of life PhD training is not an individual but rather a "team sport". The completion of my dissertation would not have been possible without the unrelenting support and guidance I received from my supervisors, colleagues, family and friends.

I would like to extend my most sincere gratitude to my main supervisor **Mahbubhul Alam** for generously sharing his wisdom on science and life and patiently guiding me through the "treacherous path" of doctoral education.

I am deeply indebted to my co-supervisor **Bassem Abdel Samad** for his incessant support and invaluable help in finding elegant solutions to complex problems.

I would like to thank my co-supervisor **Lars-Åke Brodin** for his generous support and guidance throughout the years of PhD.

I am extremely grateful to my co-author **Reidar Winter** for introducing me to the intriguing world of advanced echocardiography and for unselfishly sharing his vast knowledge, which has been such a great source of intellectual inspiration through my training.

My coauthor and friend, **Jonas Johnson** for introducing me to GHLab and CSD. **Jonas**, your "high tech" technical and scientific skills are truly inspiring

May coauthors **Magnus Dalén**, **Ulrik Sartipy** and **Peter Svenarud** for fruitful collaboration. **Magnus** thank you for all useful suggestions and guidance with the thesis.

I would like to thank my mentor **Leif Svensson,** for sharing his knowledge and enthusiasm.

I would like to extend special thanks to **Niklas Storck** for outstanding leadership, radiant optimism and his brilliant ability to think outside the box.

Also I would like to gratefully acknowledge **PA Dahlberg** for his excellent effort to forge a fertile research environment at St Görans Hospital as head of the department of Research and Development "FoU". **Anna Norhammar** chairman of "FoU", for her kindness and generosity to provide constructive

advice on how to best structure my research activities, and **Andres Byström-head of Radiology and clinical physiology department-,** for his encouragement and support.

Karin Malmqvist- head of department of cardiology Karin Malmqvist, for being the quintessential role model for leadership and being a remarkably strong woman**.**

I cannot thank enough to my friend **Nassrin Wandy** for her selfless help to find ingenuous solutions to overcome practical problems and for sharing her positive outlook on life, which tends to rub off on everyone around.

Thanks should also go to **Hans Persson, Håkan Wallen and Thomas Kahan** for being always approachable, providing me with insightful suggestions and not least for inspiring me to embark on the road of academic training.

Many thanks to **Faris Alkhalili** for generous support and source of inspiration.

I am indeed thankful to **Andrea Gomes-Bernardes** for contribution to paper No III and **Diogo Dias Da Silva Fouto** for superb help.

Malin Bauer for her warm, reassuring presence and demonstrating me the feasibility to create a perfect harmony between work and personal life.

Carina Fogelberg Varttinen and **Monika Rådestad** for sharing great laughs and making sure I take some much-needed breaks during my thesis write up at the "FoU" Department.

I had the privilege to work and share great times with my lovely colleagues throughout the years. Thank you **Peter Thermaenius, Mohamed Yousry, Henrik Hedskog, Jan Svedenhag, Ann Ekman, Anna Gustafsson, Agneta Dahlberg-Åkerman,** and all other **colleagues** at the echocardiography lab for making our work such a fun place to be at.

I would also like to thank my dear friend **Maria Myrin** for sharing such joyful times during our residency years in cardiology and beyond.

Thanks also should go to my friends, **Kelsi Cross**, **Sheida Kharrazi**, **Naser Abbasi,** and **Kristin Olsen Broksby** who made our stay in Portland such a wonderful experience.

My success would not have been possible without the incessant nurturing and support by my family.

I would like to extend my deepest gratitude to my mother **Esmat Seyedi** who has always been an unwavering source of love, energy and inspiration through my life.

My father, **Hassan Hashemi** for being my moral compass and teaching me to never give up fighting.

My brother **Amir** for his endless love and selfless support –without your support I could never have become a physician.

My sisters, **Jamileh and Shilan** and their husbands **Ismael** and **Kadir**, for their unconditional love and support and profound belief in my abilities.

My uncle, **Shahab Seyedi** for being the best uncle in the world during my upbringing in Kurdistan.

The love of my life **Jan,** and my beautiful precious daughters **Hannah** and **Julia**-you all are the greatest source of joy and meaning in my life.

9 REFERENCES

1. Curie J CP. Sur l'electricite´ polaire dans les cristaus he´mie`dres a` faces incline´es. Compt Rend Se´ances Acad Sci. 1880;91:383-9.

2. Fraser AG. Inge Edler and the origins of clinical echocardiography. Eur J Echocardiogr. 2001;2(1):3-5.

3. St John Sutton M, Pfeffer MA, Moye L, Plappert T, Rouleau JL, Lamas G, et al. Cardiovascular death and left ventricular remodeling two years after myocardial infarction: baseline predictors and impact of long-term use of captopril: information from the Survival and Ventricular Enlargement (SAVE) trial. Circulation. 1997;96(10):3294-9.

4. Oh JK SJ, Tajik JA. The echo manual. 3rd Edition: Lippincott Williams & Wilkins

5. McDicken WN, Sutherland GR, Moran CM, Gordon LN. Colour Doppler velocity imaging of the myocardium. Ultrasound Med Biol. 1992;18(6-7):651-4.

6. Sutherland GR, Bijnens B, McDicken WN. Tissue Doppler Echocardiography: Historical Perspective and Technological Considerations. Echocardiography. 1999;16(5):445-53.

7. Manouras A, Shahgaldi K, Winter R, Nowak J, Brodin LA. Comparison between colour-coded and spectral tissue Doppler measurements of systolic and diastolic myocardial velocities: effect of temporal filtering and offline gain setting. Eur J Echocardiogr. 2009;10(3):406-13.

8. Correale M, Totaro A, Ieva R, Ferraretti A, Musaico F, Di Biase M. Tissue Doppler imaging in coronary artery diseases and heart failure. Curr Cardiol Rev. 2012;8(1):43-53.

9. Lang RM, Badano LP, Mor-Avi V, Afilalo J, Armstrong A, Ernande L, et al. Recommendations for cardiac chamber quantification by echocardiography in adults: an update from the American Society of Echocardiography and the European Association of Cardiovascular Imaging. Eur Heart J Cardiovasc Imaging. 2015;16(3):233-70.

10. Buckberg GD, Hoffman JI, Coghlan HC, Nanda NC. Ventricular structure-function relations in health and disease: Part I. The normal heart. Eur J Cardiothorac Surg. 2015;47(4):587-601.

11. Torrent-Guasp F, Ballester M, Buckberg GD, Carreras F, Flotats A, Carrio I, et al. Spatial orientation of the ventricular muscle band: physiologic contribution and surgical implications. J Thorac Cardiovasc Surg. 2001;122(2):389-92.

12. Sengupta PP, Krishnamoorthy VK, Korinek J, Narula J, Vannan MA, Lester SJ, et al. Left ventricular form and function revisited: applied translational science to cardiovascular ultrasound imaging. J Am Soc Echocardiogr. 2007;20(5):539-51.

13. Solomon SD, Anavekar N, Skali H, McMurray JJ, Swedberg K, Yusuf S, et al. Influence of ejection fraction on cardiovascular outcomes in a broad spectrum of heart failure patients. Circulation. 2005;112(24):3738-44.

14. Lindqvist P, Waldenstrom A, Wikstrom G, Kazzam E. Potential use of isovolumic contraction velocity in assessment of left ventricular contractility in man: A simultaneous pulsed Doppler tissue imaging and cardiac catheterization study. Eur J Echocardiogr. 2007;8(4):252-8.

15. Edvardsen T, Urheim S, Skulstad H, Steine K, Ihlen H, Smiseth OA. Quantification of left ventricular systolic function by tissue Doppler echocardiography: added value of measuring pre- and postejection velocities in ischemic myocardium. Circulation. 2002;105(17):2071-7.

16. Yip G, Wang M, Zhang Y, Fung JW, Ho PY, Sanderson JE. Left ventricular long axis function in diastolic heart failure is reduced in both diastole and systole: time for a redefinition? Heart. 2002;87(2):121-5.

17. Zaborska B, Makowska E, Pilichowska E, Maciejewski P, Bednarz B, Wasek W, et al. The diagnostic and prognostic value of right ventricular myocardial velocities in inferior myocardial infarction treated with primary percutaneous intervention. Kardiol Pol. 2011;69(10):1054-61.

18. Edvardsen T, Gerber BL, Garot J, Bluemke DA, Lima JA, Smiseth OA. Quantitative assessment of intrinsic regional myocardial deformation by Doppler strain rate echocardiography in humans: validation against three-dimensional tagged magnetic resonance imaging. Circulation. 2002;106(1):50-6.

19. Reisner SA, Lysyansky P, Agmon Y, Mutlak D, Lessick J, Friedman Z. Global longitudinal strain: a novel index of left ventricular systolic function. J Am Soc Echocardiogr. 2004;17(6):630-3.

20. Voigt JU, Pedrizzetti G, Lysyansky P, Marwick TH, Houle H, Baumann R, et al. Definitions for a common standard for 2D speckle tracking echocardiography: consensus document of the EACVI/ASE/Industry Task Force to standardize deformation imaging. Eur Heart J Cardiovasc Imaging. 2015;16(1):1-11.

21. Collier P, Phelan D, Klein A. A Test in Context: Myocardial Strain Measured by Speckle-Tracking Echocardiography. J Am Coll Cardiol. 2017;69(8):1043-56.

22. Farsalinos KE, Daraban AM, Unlu S, Thomas JD, Badano LP, Voigt JU. Head-to-Head Comparison of Global Longitudinal Strain Measurements among Nine Different Vendors: The EACVI/ASE Inter-Vendor Comparison Study. J Am Soc Echocardiogr. 2015;28(10):1171-81, e2.

23. Tei C, Nishimura RA, Seward JB, Tajik AJ. Noninvasive Doppler-derived myocardial performance index: correlation with simultaneous measurements of cardiac catheterization measurements. J Am Soc Echocardiogr. 1997;10(2):169-78.

24. Nagueh SF, Smiseth OA, Appleton CP, Byrd BF, 3rd, Dokainish H, Edvardsen T, et al. Recommendations for the Evaluation of Left Ventricular Diastolic Function by Echocardiography: An Update from the American Society of Echocardiography and the European Association of Cardiovascular Imaging. Eur Heart J Cardiovasc Imaging. 2016;17(12):1321-60.

25. Weissler AM, Harris WS, Schoenfeld CD. Systolic time intervals in heart failure in man. Circulation. 1968;37(2):149-59.

26. Weissler AM, Harris WS, Schoenfeld CD. Bedside technics for the evaluation of ventricular function in man. Am J Cardiol. 1969;23(4):577-83.

27. Ahmed SS, Levinson GE, Schwartz CJ, Ettinger PO. Systolic time intervals as measures of the contractile state of the left ventricular myocardium in man. Circulation. 1972;46(3):559-71.

28. Mancini GB, Costello D, Bhargava V, Lew W, LeWinter M, Karliner JS. The isovolumic index: a new noninvasive approach to the assessment of left ventricular function in man. Am J Cardiol. 1982;50(6):1401-8.

29. Johnson AD, O'Rourke RA, Karliner JS, Burian C. Effect of myocardial revascularization on systolic time intervals in patients with left ventricular dysfunction. Circulation. 1972;45(1 Suppl):I91-6.

30. Hirschfeld S, Meyer R, Schwartz DC, Korfhagen J, Kaplan S. Measurement of right and left ventricular systolic time intervals by echocardiography. Circulation. 1975;51(2):304-9.

31. Stefadouros MA, Witham AC. Systolic time intervals by echocardiography. Circulation. 1975;51(1):114-7.

32. Lewis BS, Lewis N, Sapoznikov D, Gotsman MS. Isovolumic relaxation period in man. Am Heart J. 1980;100(4):490-9.

33. Mancini GB, Friedman HZ, Hramiec JE, DeBoe SF. The hemodynamic determinants of the isovolumic index. Am Heart J. 1986;112(4):791-9.

34. Tei C, Ling LH, Hodge DO, Bailey KR, Oh JK, Rodeheffer RJ, et al. New index of combined systolic and diastolic myocardial performance: a simple and reproducible measure of cardiac function--a study in normals and dilated cardiomyopathy. J Cardiol. 1995;26(6):357-66.

35. Tei C, Dujardin KS, Hodge DO, Kyle RA, Tajik AJ, Seward JB. Doppler index combining systolic and diastolic myocardial performance: clinical value in cardiac amyloidosis. J Am Coll Cardiol. 1996;28(3):658-64.

36. Correale M, Totaro A, Ieva R, Brunetti ND, Di Biase M. Time intervals and myocardial performance index by tissue Doppler imaging. Intern Emerg Med. 2011;6(5):393-402.

37. Moller JE, Poulsen SH, Egstrup K. Effect of preload alternations on a new Doppler echocardiographic index of combined systolic and diastolic performance. J Am Soc Echocardiogr. 1999;12(12):1065-72.

38. Sohn DW, Chai IH, Lee DJ, Kim HC, Kim HS, Oh BH, et al. Assessment of mitral annulus velocity by Doppler tissue imaging in the evaluation of left ventricular diastolic function. J Am Coll Cardiol. 1997;30(2):474-80.

39. Tekten T, Onbasili AO, Ceyhan C, Unal S, Discigil B. Novel approach to measure myocardial performance index: pulsed-wave tissue Doppler echocardiography. Echocardiography. 2003;20(6):503-10.

40. Gaibazzi N, Petrucci N, Ziacchi V. Left ventricle myocardial performance index derived either by conventional method or mitral annulus tissue-Doppler: a comparison study in healthy subjects and subjects with heart failure. J Am Soc Echocardiogr. 2005;18(12):1270-6.

41. Biering-Sorensen T, Mogelvang R, Schnohr P, Jensen JS. Cardiac Time Intervals Measured by Tissue Doppler Imaging M-mode: Association With Hypertension, Left Ventricular Geometry, and Future Ischemic Cardiovascular Diseases. Journal of the American Heart Association. 2016;5(1).

42. Biering-Sorensen T, Mogelvang R, de Knegt MC, Olsen FJ, Galatius S, Jensen JS. Cardiac Time Intervals by Tissue Doppler Imaging M-Mode: Normal Values and Association with Established Echocardiographic and Invasive Measures of Systolic and Diastolic Function. PLoS One. 2016;11(4):e0153636.

43. Larsson M, Bjallmark A, Johnson J, Winter R, Brodin LA, Lundback S. State diagrams of the heart--a new approach to describing cardiac mechanics. Cardiovasc Ultrasound. 2009;7:22.

44. Lundbäck S, Johnson J iGHAS, SE), assignee. State space model of a heart. United States 2012., inventors.

45. Surkova E, Peluso D, Kasprzak JD, Badano LP. Use of novel echocardiographic techniques to assess right ventricular geometry and function. Kardiol Pol. 2016;74(6):507-22.

46. Haddad F, Hunt SA, Rosenthal DN, Murphy DJ. Right ventricular function in cardiovascular disease, part I: Anatomy, physiology, aging, and functional assessment of the right ventricle. Circulation. 2008;117(11):1436-48.

47. Dandel M, Hetzer R. Echocardiographic assessment of the right ventricle: Impact of the distinctly load dependency of its size, geometry and performance. Int J Cardiol. 2016;221:1132-42.

48. Rudski LG, Lai WW, Afilalo J, Hua L, Handschumacher MD, Chandrasekaran K, et al. Guidelines for the echocardiographic assessment of the right heart in adults: a report from the American Society of Echocardiography endorsed by the European Association of Echocardiography, a registered branch of the European Society of Cardiology, and the Canadian Society of Echocardiography. J Am Soc Echocardiogr. 2010;23(7):685-713; quiz 86-8.

49. van der Zwaan HB, Helbing WA, McGhie JS, Geleijnse ML, Luijnenburg SE, Roos-Hesselink JW, et al. Clinical value of real-time three-dimensional echocardiography for right ventricular quantification in congenital heart disease: validation with cardiac magnetic resonance imaging. J Am Soc Echocardiogr. 2010;23(2):134-40.

50. Murninkas D, Alba AC, Delgado D, McDonald M, Billia F, Chan WS, et al. Right ventricular function and prognosis in stable heart failure patients. J Card Fail. 2014;20(5):343-9.

51. Kaul S, Tei C, Hopkins JM, Shah PM. Assessment of right ventricular function using two-dimensional echocardiography. Am Heart J. 1984;107(3):526-31.

52. Sato T, Tsujino I, Oyama-Manabe N, Ohira H, Ito YM, Sugimori H, et al. Simple prediction of right ventricular ejection fraction using tricuspid annular plane systolic excursion in pulmonary hypertension. Int J Cardiovasc Imaging. 2013;29(8):1799-805.

53. Lang RM, Bierig M, Devereux RB, Flachskampf FA, Foster E, Pellikka PA, et al. Recommendations for chamber quantification: a report from the American Society of Echocardiography's Guidelines and Standards Committee and the Chamber Quantification Writing Group, developed in conjunction with the European Association of Echocardiography, a branch of the European Society of Cardiology. J Am Soc Echocardiogr. 2005;18(12):1440-63.

54. Samad BA, Alam M, Jensen-Urstad K. Prognostic impact of right ventricular involvement as assessed by tricuspid annular motion in patients with acute myocardial infarction. Am J Cardiol. 2002;90(7):778-81.

55. Meluzin J, Spinarova L, Bakala J, Toman J, Krejci J, Hude P, et al. Pulsed Doppler tissue imaging of the velocity of tricuspid annular systolic motion; a new, rapid, and non-invasive method of evaluating right ventricular systolic function. Eur Heart J. 2001;22(4):340-8.

56. Innelli P, Esposito R, Olibet M, Nistri S, Galderisi M. The impact of ageing on right ventricular longitudinal function in healthy subjects: a pulsed tissue Doppler study. Eur J Echocardiogr. 2009;10(4):491-8.

57. Focardi M, Cameli M, Carbone SF, Massoni A, De Vito R, Lisi M, et al. Traditional and innovative echocardiographic parameters for the analysis of right ventricular performance in

comparison with cardiac magnetic resonance. Eur Heart J Cardiovasc Imaging. 2015;16(1):47-52.

58. Maslow AD, Regan MM, Panzica P, Heindel S, Mashikian J, Comunale ME. Precardiopulmonary bypass right ventricular function is associated with poor outcome after coronary artery bypass grafting in patients with severe left ventricular systolic dysfunction. Anesth Analg. 2002;95(6):1507-18, table of contents.

59. Zornoff LAM, Skali H, Pfeffer MA, St. John Sutton M, Rouleau JL, Lamas GA, et al. Right ventricular dysfunction and risk of heart failure and mortality after myocardial infarction. J Am Coll Cardiol. 2002;39(9):1450-5.

60. Szymczyk E, Lipiec P, Plewka M, Bialas M, Olszewska M, Rozwadowska N, et al. Feasibility of strain and strain rate evaluation by two-dimensional speckle tracking in murine model of myocardial infarction: comparison with tissue Doppler echocardiography. J Cardiovasc Med (Hagerstown). 2013;14(2):136-43.

61. Teske AJ, De Boeck BW, Olimulder M, Prakken NH, Doevendans PA, Cramer MJ. Echocardiographic assessment of regional right ventricular function: a head-to-head comparison between 2-dimensional and tissue Doppler-derived strain analysis. J Am Soc Echocardiogr. 2008;21(3):275-83.

62. Verhaert D, Mullens W, Borowski A, Popovic ZB, Curtin RJ, Thomas JD, et al. Right ventricular response to intensive medical therapy in advanced decompensated heart failure. Circ Heart Fail. 2010;3(3):340-6.

63. Antoni ML, Scherptong RW, Atary JZ, Boersma E, Holman ER, van der Wall EE, et al. Prognostic value of right ventricular function in patients after acute myocardial infarction treated with primary percutaneous coronary intervention. Circ Cardiovasc Imaging. 2010;3(3):264-71.

64. Cappelli F, Porciani MC, Bergesio F, Perlini S, Attana P, Moggi Pignone A, et al. Right ventricular function in AL amyloidosis: characteristics and prognostic implication. Eur Heart J Cardiovasc Imaging. 2012;13(5):416-22.

65. Shukla M, Park JH, Thomas JD, Delgado V, Bax JJ, Kane GC, et al. Prognostic Value of Right Ventricular Strain Using Speckle-Tracking Echocardiography in Pulmonary Hypertension: A Systematic Review and Meta-analysis. Can J Cardiol. 2018;34(8):1069-78.

66. Yu HC, Sanderson JE. Different prognostic significance of right and left ventricular diastolic dysfunction in heart failure. Clin Cardiol. 1999;22(8):504-12.

67. Maeda K, Tsutamoto T, Wada A, Hisanaga T, Kinoshita M. Plasma brain natriuretic peptide as a biochemical marker of high left ventricular end-diastolic pressure in patients with symptomatic left ventricular dysfunction. Am Heart J. 1998;135(5 Pt 1):825-32.

68. Weber M, Hamm C. Role of B-type natriuretic peptide (BNP) and NT-proBNP in clinical routine. Heart. 2006;92(6):843-9.

69. Wang TJ, Larson MG, Levy D, Leip EP, Benjamin EJ, Wilson PW, et al. Impact of age and sex on plasma natriuretic peptide levels in healthy adults. Am J Cardiol. 2002;90(3):254-8.

70. Li P, Luo Y, Chen YM. B-type natriuretic peptide-guided chronic heart failure therapy: a meta-analysis of 11 randomised controlled trials. Heart Lung Circ. 2013;22(10):852-60.

71. Ponikowski P, Voors AA, Anker SD, Bueno H, Cleland JG, Coats AJ, et al. 2016 ESC Guidelines for the diagnosis and treatment of acute and chronic heart failure: The Task Force for

the diagnosis and treatment of acute and chronic heart failure of the European Society of Cardiology (ESC). Developed with the special contribution of the Heart Failure Association (HFA) of the ESC. Eur J Heart Fail. 2016;18(8):891-975.

72. Anand IS, Fisher LD, Chiang YT, Latini R, Masson S, Maggioni AP, et al. Changes in brain natriuretic peptide and norepinephrine over time and mortality and morbidity in the Valsartan Heart Failure Trial (Val-HeFT). Circulation. 2003;107(9):1278-83.

73. Richards AM, Nicholls MG, Espiner EA, Lainchbury JG, Troughton RW, Elliott J, et al. B-type natriuretic peptides and ejection fraction for prognosis after myocardial infarction. Circulation. 2003;107(22):2786-92.

74. Gerber IL, Stewart RA, Legget ME, West TM, French RL, Sutton TM, et al. Increased plasma natriuretic peptide levels reflect symptom onset in aortic stenosis. Circulation. 2003;107(14):1884-90.

75. Sicari R, Nihoyannopoulos P, Evangelista A, Kasprzak J, Lancellotti P, Poldermans D, et al. Stress echocardiography expert consensus statement: European Association of Echocardiography (EAE) (a registered branch of the ESC). Eur J Echocardiogr. 2008;9(4):415-37.

76. Fletcher GF, Froelicher VF, Hartley LH, Haskell WL, Pollock ML. Exercise standards. A statement for health professionals from the American Heart Association. Circulation. 1990;82(6):2286-322.

77. Gibbons RJ, Balady GJ, Beasley JW, Bricker JT, Duvernoy WF, Froelicher VF, et al. ACC/AHA Guidelines for Exercise Testing. A report of the American College of Cardiology/American Heart Association Task Force on Practice Guidelines (Committee on Exercise Testing). J Am Coll Cardiol. 1997;30(1):260-311.

78. Lundbäck S, Johnson J, Bergholm F, inventor; Inovacor AB (Stockholm, SE), assignee. A cardiac state monitoring system. Sweden 2016., inventors.

79. Unsworth B, Casula RP, Kyriacou AA, Yadav H, Chukwuemeka A, Cherian A, et al. The right ventricular annular velocity reduction caused by coronary artery bypass graft surgery occurs at the moment of pericardial incision. Am Heart J. 2010;159(2):314-22.

80. Steffen HJ, Kalverkamp S, Zayat R, Autschbach R, Spillner JW, Hagendorff A, et al. Is Systolic Right Ventricular Function Reduced after Thoracic Non-Cardiac Surgery? A Propensity Matched Echocardiographic Analysis. Ann Thorac Cardiovasc Surg. 2018.

81. Giusca S, Dambrauskaite V, Scheurwegs C, D'Hooge J, Claus P, Herbots L, et al. Deformation imaging describes right ventricular function better than longitudinal displacement of the tricuspid ring. Heart. 2010;96(4):281-8.

82. Lindqvist P, Waldenstrom A, Henein M, Morner S, Kazzam E. Regional and global right ventricular function in healthy individuals aged 20-90 years: a pulsed Doppler tissue imaging study: Umea General Population Heart Study. Echocardiography. 2005;22(4):305-14.

83. Kempny A, Diller GP, Kaleschke G, Orwat S, Funke A, Schmidt R, et al. Impact of transcatheter aortic valve implantation or surgical aortic valve replacement on right ventricular function. Heart. 2012;98(17):1299-304.

84. Tamborini G, Muratori M, Brusoni D, Celeste F, Maffessanti F, Caiani EG, et al. Is right ventricular systolic function reduced after cardiac surgery? A two- and three-dimensional echocardiographic study. Eur J Echocardiogr. 2009;10(5):630-4.

85. Raina A, Vaidya A, Gertz ZM, Susan C, Forfia PR. Marked changes in right ventricular contractile pattern after cardiothoracic surgery: implications for post-surgical assessment of right ventricular function. J Heart Lung Transplant. 2013;32(8):777-83.

86. Bergsma TM, Grandjean JG, Voors AA, Boonstra PW, den Heyer P, Ebels T. Low recurrence of angina pectoris after coronary artery bypass graft surgery with bilateral internal thoracic and right gastroepiploic arteries. Circulation. 1998;97(24):2402-5.

87. Brorsson B, Lindvall B, Bernstein SJ, Aberg T. CABG in chronic stable angina pectoris patients: indications and outcomes (SECOR/SBU). Swedish Societies for Cardiology, Thoracic Radiology and Thoracic surgery/Swedish Council for Technology Assessment in Health Care. Eur J Cardiothorac Surg. 1997;12(5):746-52.

88. Herlitz J, Karlson BW, Sjoland H, Albertsson P, Brandrup-Wognsen G, Hartford M, et al. Physical activity, symptoms of chest pain and dyspnea in patients with ischemic heart disease in relation to age before and two years after coronary artery bypass grafting. J Cardiovasc Surg (Torino). 2001;42(2):165-73.

89. Okada DR, Rahmouni HW, Herrmann HC, Bavaria JE, Forfia PR, Han Y. Assessment of right ventricular function by transthoracic echocardiography following aortic valve replacement. Echocardiography. 2014;31(5):552-7.

90. D'Hooge J, Heimdal A, Jamal F, Kukulski T, Bijnens B, Rademakers F, et al. Regional strain and strain rate measurements by cardiac ultrasound: principles, implementation and limitations. Eur J Echocardiogr. 2000;1(3):154-70.

91. Missant C, Rex S, Claus P, Mertens L, Wouters PF. Load-sensitivity of regional tissue deformation in the right ventricle: isovolumic versus ejection-phase indices of contractility. Heart. 2008;94(4):e15.

92. Rizzello V, Poldermans D, Biagini E, Schinkel AF, van Domburg R, Elhendy A, et al. Improvement of stress LVEF rather than rest LVEF after coronary revascularisation in patients with ischaemic cardiomyopathy and viable myocardium. Heart. 2005;91(3):319-23.

93. Bax JJ, Poldermans D, Elhendy A, Cornel JH, Boersma E, Rambaldi R, et al. Improvement of left ventricular ejection fraction, heart failure symptoms and prognosis after revascularization in patients with chronic coronary artery disease and viable myocardium detected by dobutamine stress echocardiography. J Am Coll Cardiol. 1999;34(1):163-9.

94. Bax JJ, Wijns W, Cornel JH, Visser FC, Boersma E, Fioretti PM. Accuracy of Currently Available Techniques for Prediction of Functional Recovery After Revascularization in Patients With Left Ventricular Dysfunction Due to Chronic Coronary Artery Disease: Comparison of Pooled Data. J Am Coll Cardiol. 1997;30(6):1451-60.

95. Beanlands RSB, Ruddy TD, deKemp RA, Iwanochko RM, Coates G, Freeman M, et al. Positron emission tomography and recovery following revascularization (PARR-1): the importance of scar and the development of a prediction rule for the degree of recovery of left ventricular function. J Am Coll Cardiol. 2002;40(10):1735-43.

96. Fitzgibbon GM, Kafka HP, Leach AJ, Keon WJ, Hooper GD, Burton JR. Coronary bypass graft fate and patient outcome: Angiographic follow-up of 5,065 grafts related to survival and reoperation in 1,388 patients during 25 years. J Am Coll Cardiol. 1996;28(3):616-26.

97. Nozohoor S, Nilsson J, Algotsson L, Sjogren J. Postoperative increase in B-type natriuretic peptide levels predicts adverse outcome after cardiac surgery. J Cardiothorac Vasc Anesth. 2011;25(3):469-75.

98. Fellahi JL, Daccache G, Makroum Y, Massetti M, Gerard JL, Hanouz JL. The prognostic value of B-type natriuretic peptide after cardiac surgery: a comparative study between coronary artery bypass graft surgery and aortic valve replacement. J Cardiothorac Vasc Anesth. 2012;26(4):624-30.

99. Fox AA, Nascimben L, Body SC, Collard CD, Mitani AA, Liu KY, et al. Increased perioperative b-type natriuretic peptide associates with heart failure hospitalization or heart failure death after coronary artery bypass graft surgery. Anesthesiology. 2013;119(2):284-94.

100. Vanoverschelde JL, Depre C, Gerber BL, Borgers M, Wijns W, Robert A, et al. Time course of functional recovery after coronary artery bypass graft surgery in patients with chronic left ventricular ischemic dysfunction. Am J Cardiol. 2000;85(12):1432-9.